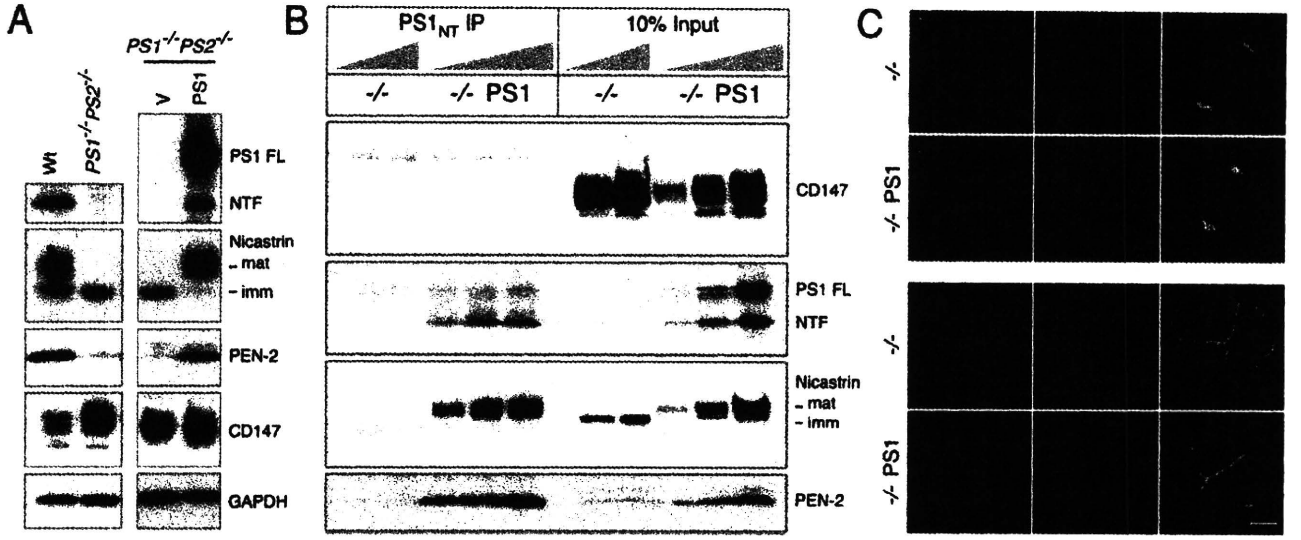

FIGURE 1. **Subcellular localization of CD147 in the absence of γ-secretase subunit expression.** *A*, comparison of the steady-state levels of CD147 and γ-secretase subunits. Total cell lysates from WT and $PS1^{-/-}/PS2^{-/-}$ MEFs and $PS1^{-/-}/PS2^{-/-}$ pools stably transduced with retrovirus harboring empty vector or human PS1 cDNA were probed with the indicated antibodies. Similar results were obtained in two independent pools of stably transduced cells. *FL*, full-length; *mat*, mature; *imm*, immature; *GAPDH*, glyceraldehyde-3-phosphate dehydrogenase. *B*, co-immunoprecipitation analysis of CD147 with γ-secretase subunits. $PS1^{-/-}/PS2^{-/-}$ MEFs stably overexpressing empty vector or human PS1 were lysed in 1% CHAPSO, co-immunoprecipitated using the $PS1_{NT}$ antibody as described under "Experimental Procedures," and probed with the indicated antibodies. Note that the endogenous γ-secretase components nicastrin and PEN-2 co-immunoprecipitated with PS1; CD147 was not detected as part of the immunoprecipitated complex. Similar results were obtained in co-immunoprecipitation analysis of mouse N2a neuroblastoma cells and HEK293 cells. *C*, analysis of the indicated $PS1^{-/-}/PS2^{-/-}$ MEFs pools by double immunofluorescence staining with anti-CD147 antibody (*green*) and antibody against GM130 (*cis*-Golgi) or cadherin (cell surface) (*red*). The *right panels* represent image overlays. *Scale bar* = 10 μm. These images are representative of two independent experiments, and similar results were observed in analysis of $NCT^{-/-}$ MEFs.

Assay for Aβ-degrading Metalloproteases in Culture Medium—The culture medium from either HEK293 cells or HEK293 cells stably overexpressing CD147 was incubated with metalloprotease-specific inhibitors to indirectly identify the type of Aβ-degrading metalloproteases induced by CD147. 30 μl of conditioned medium from HEKswe cells (as the source of secreted Aβ) was incubated overnight in a 37 °C incubator with 30 μl of conditioned medium from either naïve HEK293 cells or CD147-overexpressing cells. To inhibit the degradation of Aβ during the incubation, different protease inhibitors were included as indicated. The final concentrations of the inhibitors used were 10 mM 1,10-phenanthroline (Aldrich), 5 mM EDTA, 2.5 μM thiorphan (Sigma), 10 μM Nap (a kind gift from Dr. Malcolm Leissring), 100 μM actinonin, and 50 μM GM6001 (BIOMOL International). Aβ remaining intact at the end of the incubation period was analyzed by Western blotting and quantified by enzyme-linked immunosorbent assay (ELISA) following the manufacturer's protocol (Invitrogen).

Zymography Analysis of Conditioned Medium—6 μl of conditioned medium from either naïve HEK293 cells or CD147-overexpressing cells was mixed with nonreducing sample buffer and fractionated on a 7.5% SDS gel containing 0.1% gelatin. After electrophoresis, the gel was developed and stained with Coomassie Blue as described previously (29).

RESULTS

Stability of CD147 Is Not Affected in the Absence of γ-Secretase Core Components—If CD147 is a *bona fide* component of γ-secretase, one would anticipate that the behavior of the polypeptide with respect to regulated stability would be similar to that already established for other core components of the complex, *i.e.* that the stability and maturation of γ-secretase subunits are co-regulated. To examine the stability of CD147 in cells lacking PS1/PS2, we employed fibroblasts derived from $PS1^{-/-}/PS2^{-/-}$ embryos and their wild-type (WT) littermates. As reported previously (9, 12), maturation of endogenous nicastrin was impaired, and the steady-state levels of endogenous PEN-2 were significantly reduced in $PS1^{-/-}/PS2^{-/-}$ MEFs compared with WT MEFs. In contrast and for reasons that are presently not clear, endogenous CD147 levels were elevated in $PS1^{-/-}/PS2^{-/-}$ MEFs (Fig. 1*A*, *first* and *second lanes*). To address the possibility that the observed difference in the levels of CD147 may be a result of cell-to-cell variation in the MEFs analyzed, we generated stable pools of $PS1^{-/-}/PS2^{-/-}$ MEFs overexpressing human PS1 by retroviral infection. Stable expression of PS1 in $PS1^{-/-}/PS2^{-/-}$ cells restored mature glycosylation of nicastrin and stabilized PEN-2, but did not markedly affect CD147 protein levels (Fig. 1*A*, *third* and *fourth lanes*). Similarly, CD147 levels were not reduced in $NCT^{-/-}$ or $APH1ab^{-/-}$ MEFs compared with WT MEFs, as would be expected if this polypeptide were a γ-secretase component (data not shown). Thus, the stability of CD147 is not co-regulated in a manner such as PS1, nicastrin, APH1, and PEN-2, indicating that CD147 is unlikely to be an integral subunit of the γ-secretase complex.

To further confirm the above findings, we also performed co-immunoprecipitation analyses in $PS1^{-/-}/PS2^{-/-}$ MEFs. Aliquots of 1% CHAPSO lysates of $PS1^{-/-}/PS2^{-/-}$ MEFs stably overexpressing human PS1 were immunoprecipitated with the PS1 N-terminal antiserum $PS1_{NT}$. The resulting immune complexes were subjected to Western blot analysis with anti-

Downloaded from www.jbc.org at RIKEN LIB on February 16, 2009

CD147 antibody. The blots were then sequentially reprobed with antibodies against nicastrin, PEN-2, and PS1 CTFs. The results show efficient co-immunoprecipitation of endogenous γ-secretase core components nicastrin and PEN-2 with human PS1 expressed in $PS1^{-/-}/PS2^{-/-}$ MEFs (Fig. 1*B*). In contrast, CD147 failed to co-immunoprecipitate with PS1, nicastrin, and PEN-2 under these conditions (Fig. 1*B*). Thus, we conclude that CD147 is not a stoichiometric subunit of the γ-secretase complex.

Subcellular Localization of CD147 Is Unaffected by the Absence of γ-Secretase Core Components—Several studies have demonstrated that the integral components of γ-secretase cooperatively mature and exit the ER. CD147 is a type I membrane protein that is principally localized to the cell surface (30). To examine the subcellular localization of CD147 in the absence of γ-secretase core components, we performed confocal microscopic analysis of CD147 in $PS1^{-/-}/PS2^{-/-}$ and $NCT^{-/-}$ MEFs. There was no observable difference in the overall distribution of CD147 between $PS1^{-/-}/PS2^{-/-}$ MEFs and those expressing human PS1. Co-staining with organelle markers GM130, a *cis*-Golgi-associated protein, and cadherin, a cell-surface protein, showed similar CD147 localization in the Golgi and at the cell surface (Fig. 1*C*). Similar results were obtained in $NCT^{-/-}$ cells (data not shown). Thus, the subcellular localization of CD147 is not dependent on the expression of PS1 or nicastrin.

DRM Association of CD147 and the Core Components of the γ-Secretase Complex Is Not Codependent—We and others (27, 31) have reported that the PS1 NTF and CTF, mature nicastrin, APH1, and PEN-2 are localized within detergent-insoluble membrane microdomains, which are enriched in the lipid raft markers flotillin-2 and prion protein. Interestingly, we found that the assembly of core components precedes DRM association of the γ-secretase complex. For example, in $NCT^{-/-}$ fibroblasts, the low levels of APH1 and PEN-2 that escape degradation reside in non-raft domains (27). Therefore, we investigated whether DRM association of CD147 is dependent on the presence of γ-secretase complex components. To this end, we analyzed DRM association of CD147 in $PS1^{-/-}/PS2^{-/-}$ and $NCT^{-/-}$ MEFs and compared these profiles with that of either WT MEFs or $NCT^{-/-}$ MEFs stably overexpressing nicastrin, respectively. By sucrose density gradient fractionation, we found that CD147 was enriched in Lubrol WX-resistant membrane fractions of WT MEFs (Fig. 2*A*). However, DRM association of CD147 was unchanged in $PS1^{-/-}/PS2^{-/-}$ and $NCT^{-/-}$ cells (Fig. 2). Thus, expression of γ-secretase subunits does not regulate lipid raft association of CD147.

Several lines of evidence in cell culture and mouse brain indicate that lipid raft microdomains are the principal sites of amyloidogenic processing of APP (26, 31). Therefore, we considered the possibility that the levels of CD147 might affect the association of PS1 with DRMs and thereby influence APP processing in lipid rafts. To address this issue, we prepared membranes from HEK293 cells with different levels of CD147 expression. We observed that neither elevated nor lowered expression of CD147 had a discernible effect on the DRM association of endogenous PS1 (Fig. 3). Thus, we find it implausible that CD147 modulates lipid raft localization of γ-secretase.

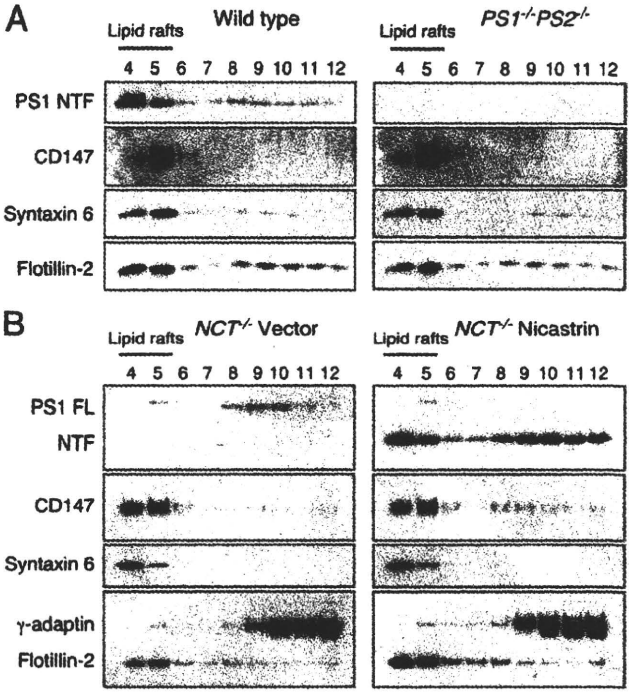

FIGURE 2. **DRM association of CD147 is not dependent on the presence of γ-secretase core components.** *A*, WT and $PS1^{-/-}/PS2^{-/-}$ MEFs were solubilized in 0.5% Lubrol WX at 4 °C for 30 min. The lysates were then subjected to flotation centrifugation on discontinuous sucrose gradients as described previously (27). The gradients were harvested from the top (fractions 1–12; top to bottom), and the distribution of PS1, CD147, syntaxin-6, and flotillin-2 was determined by fractionating 60-μl aliquots of gradient fractions 4–12. *B*, $NCT^{-/-}$ MEFs stably infected with retrovirus harboring empty vector or WT nicastrin cDNA were lysed and fractionated as described above. Note that fractions 1–3 contained no detectable signal for any protein analyzed. The raft marker flotillin-2 was recovered primarily in fractions 4 and 5, and the non-raft protein γ-adaptin was recovered in detergent-soluble fractions 9–12. The data are representative of two independent experiments; moreover, DRM fractionation was performed in WT, $NCT^{-/-}$, and $APH1ab^{-/-}$ MEFs with similar results. *FL*, full-length.

Postnatal Expression and Distribution of CD147 in Brain Show Lack of Correlation with Nicastrin—Our failure to document that CD147 levels, subcellular localization, and DRM association are co-regulated by the core components of γ-secretase in cultured cells was perplexing and prompted us to assess the expression patterns of CD147 in brain, arguably a more relevant setting. Unfortunately, little information is available pertaining to CD147 expression in brain, and hence, we sought to characterize the expression profile of CD147 relative to the γ-secretase core components PS1 and nicastrin in mouse brain during postnatal developmental stages. Western blot analyses of total brain lysates showed that CD147 protein levels were remarkably low at embryonic day 15, but readily detectable at birth. CD147 expression increased by 3.5-fold between postnatal days 0 and 7 and remained at this high level through 12 months of age (Fig. 4, *A* and *B*). A completely different expression pattern was observed for the γ-secretase core components PS1 and nicastrin, with high levels of expression occurring between embryonic day 15 and postnatal day 7 and then gradually declining after postnatal day 14 (Fig. 4, *A* and *B*). These results reveal that the developmental expression patterns

Downloaded from www.jbc.org at RIKEN LIB on February 16, 2009

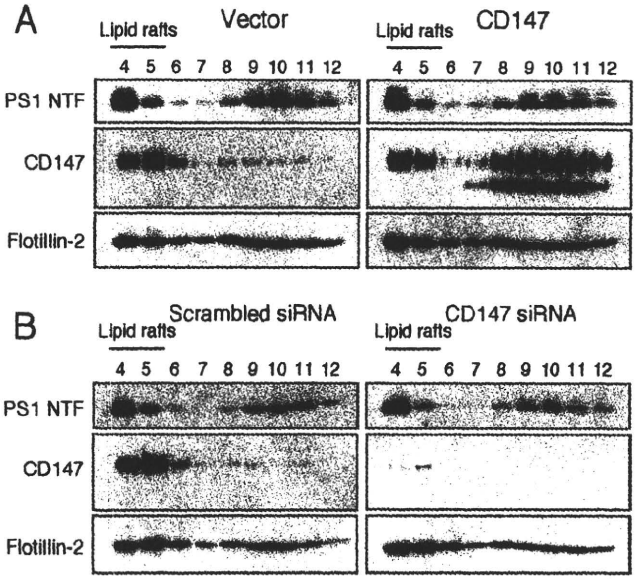

FIGURE 3. **DRM association of PS1 is not affected by CD147 overexpression or depletion.** *A*, HEK293 cells transfected with an empty vector and stably transfected cells overexpressing CD147 were lysed in 0.5% Lubrol WX and analyzed by flotation on sucrose gradients. Lipid raft localization of CD147, PS1 NTF, and flotillin-2 was analyzed by Western blotting. *B*, HEK293 cells transfected with CD147 or scrambled siRNA were fractionated as described above to analyze DRM distribution of PS1 and CD147.

of the γ-secretase core components PS1 and nicastrin do not correlate with that of CD147.

Next, we also observed remarkable differences in the cellular distributions of nicastrin and CD147 in adult mouse brain using immunohistochemical staining. We found that nicastrin immunoreactivity was restricted mainly to neuronal cell bodies throughout the cortex and to pyramidal as well as granule cells in the hippocampus (Fig. 4*C*). CD147 immunoreactivity was excluded from neuronal cell bodies, and punctate CD147 staining was seen mainly in neuronal processes. Intense CD147 staining was observed in the CA1 region of the hippocampus and upper layers of the cortex, whereas CA2 was only weakly labeled, and the dentate gyrus region was not labeled (Fig. 4*C*). The striking difference in CD147 immunoreactivity at the junction of the CA1 and CA2 regions was reproducible in all sections examined from multiple animals. The mutually exclusive pattern of nicastrin and CD147 distribution was particularly obvious in the pyramidal cell layer of the hippocampus, where nicastrin was found in the cell body and CD147 immunoreactivity was found largely in the neuronal processes within the stratum oriens, stratum radiatum, and stratum lacunosum-moleculare (Fig. 4*E*). These results do not exclude the possibility of an interaction between CD147 and γ-secretase components present at low levels in neuronal processes, but strongly suggest that CD147 is involved mainly in functions other than the regulation of the γ-secretase complex in neurons.

CD147 Depletion Increases Extracellular Aβ Independent of α- and β-Secretase Processing of APP—Consistent with the report by Zhou *et al.* (16), transfection of CD147 siRNA at increasing concentrations revealed a dose-dependent increase in Aβ levels in the medium of HEK293 cells transiently overexpressing human WT APP695 (Fig. 5*A*). In these studies, we found no significant change in the levels of full-length APP, APP CTFs, or secreted APPα (Fig. 5*A*) These results suggest that the increase in secreted Aβ associated with the depletion of CD147 expression is independent of α- and β-secretase processing of APP. To confirm these data, we analyzed the effect of siRNA-mediated knockdown of CD147 expression on secreted Aβ levels in cells stably expressing APPswe. We observed a small but consistent increase in secreted Aβ levels in cells transfected with CD147 siRNA compared with those transfected with control siRNA, whereas the steady-state levels of α- and β-CTFs remained unchanged (Fig. 5*B*). Taken together, these results indicate that siRNA-mediated depletion of CD147 expression increases the levels of Aβ in medium without significant changes in the levels of APP CTFs, the penultimate substrates of γ-secretase, hence arguing against an effect on β- or α-secretase processing of full-length APP.

In addition to the extracellular release of Aβ, γ-secretase cleavage of APP CTFs at the "ε-site" releases the APP intracellular domain (AICD) from the membrane. Similarly, ε-cleavage of Notch releases the Notch intracellular domain (NICD). To examine the potential influence of CD147 on ε-cleavage of substrates, we first asked whether depletion of CD147 has any effect on AICD production. We found that there was no quantitative difference in the levels of AICD generated by cleavage of C-terminally epitope-tagged APP (APP695-6Myc) in transfected HEK293 cells following siRNA-mediated depletion of CD147 expression (Fig. 5*C*). Furthermore, CD147 depletion had no discernible effect on the generation of the NICD following γ-secretase cleavage of N-terminally truncated Notch (mNotchΔE) at the ε-site (Fig. 5*D*). Pretreatment of transfected cells with Compound E markedly diminished the production of the AICD and NICD, establishing the specificity of these commonly used cell-based γ-secretase assays. Thus, we conclude that CD147 does not modulate ε-cleavage of substrates by the γ-secretase.

CD147 Effect on Aβ Levels Is Not Mediated through Direct Modulation of γ-Secretase Activity—CD147 has been implicated in many cellular functions, including the induction of MMPs (18) and cell-surface trafficking of the monocarboxylate transporters MCT1 and MCT4 (32). Therefore, we asked whether the influence of CD147 on extracellular Aβ levels could be mediated through direct modulation of γ-secretase, as was reported previously (16), or by an indirect mechanism unrelated to γ-secretase processing of APP β-CTFs. To this end, we asked whether we could recapitulate the cell-based findings of a role for CD147 in Aβ production in a well established *in vitro* reconstitution system that employs detergent-solubilized membranes in conjunction with a purified C100 substrate (14). The rationale for using the *in vitro* assay is that it selectively reports on Aβ production by γ-secretase cleavage of recombinant C100-FLAG substrate, thereby formally ruling out the potential influence of CD147 on trafficking of APP or the β-CTF, exocytosis or endocytosis of Aβ, and stability of extracellular Aβ, which might account for the increase in Aβ levels in the conditioned medium of CD147-depleted cells observed in both our experiments and the earlier study. As an internal control for the enzyme selectivity in this *in vitro* assay, we incubated parallel reactions with L685,458, a potent transi-

Downloaded from www.jbc.org at RIKEN LIB on February 16, 2009

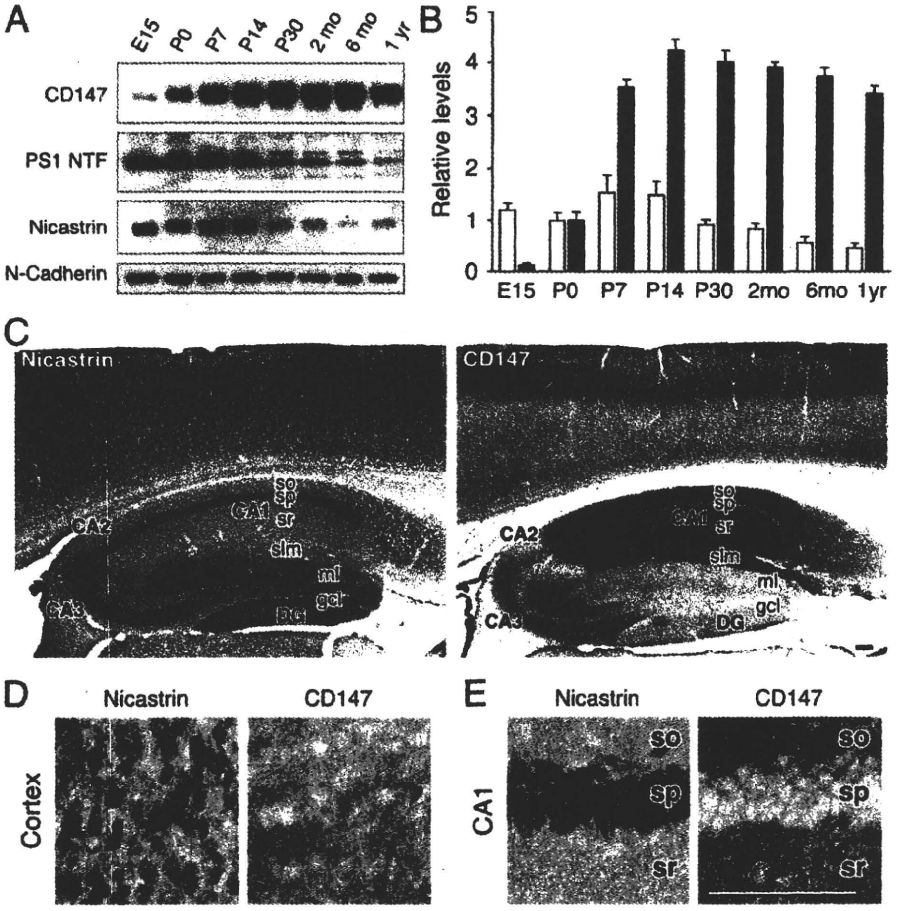

FIGURE 4. **Uncorrelated protein expression profile between CD147 and γ-secretase integral components in mouse brain.** *A*, lysates from mouse brains harvested at the indicated stages of embryonic (*E*), postnatal (*P*), and adult development were analyzed by immunoblotting. *mo*, month; *yr*, year. *B*, signal intensities of CD147 and nicastrin were determined from three independent samples and normalized to N-cadherin levels. For comparison, the normalized expression level of each protein at postnatal day 0 was set to 1, and the level of expression relative to postnatal day 0 was plotted. *C*, shown is the immunocytochemistry for nicastrin and CD147 in the hippocampus and overlying cortex of 2-month-old C57BL/6J mouse brain. *D* and *E*, higher magnifications are shown of the cortex and pyramidal cell layer in the CA1 region of the hippocampus. Nicastrin immunoreactivity was essentially restricted to neuronal cell bodies in the cortex and hippocampus, whereas CD147 immunoreactivity was excluded mainly from the cell bodies. Intense CD147 immunoreactivity was found in the CA1 stratum oriens (*so*), stratum radiatum (*sr*), and also stratum lacunosum-moleculare (*slm*). Note that anti-CD147 antibody also labeled blood vessels. *DG*, dentate gyrus; *gcl*, granule cell layer; *ml*, molecular layer; *sp*, stratum pyramidale. *Scale bar* = 100 μm. These images are representative of two independent experiments.

tion-state isostere inhibitor of γ-secretase. Surprisingly, the *in vitro* Aβ assays revealed that membranes isolated from CD147-depleted HEK293 cells did not increase Aβ production compared with those of control siRNA (Fig. 5*E*). Compared with the obvious increase in extracellular Aβ levels followed by CD147 depletion in intact cells, the results obtained from *in vitro* Aβ assays were unanticipated. The above results strongly suggest that the regulatory function of CD147 on extracellular Aβ levels is unlikely mediated through its proposed role as a regulatory subunit of the γ-secretase complex, which modulates intramembranous proteolysis of substrates.

Reduced Stability of Synthetic Aβ in Medium Conditioned by HEK293 Cells Overexpressing CD147—The series of preceding experiments failed to confirm the proposal that CD147 plays a role in Aβ production by modulating γ-secretase levels and activity. Hence, we were left with the scenario that CD147 modulates extracellular Aβ levels via an indirect mechanism that engages a known functional attribute of the polypeptide. Among the diverse functions assigned to CD147 in diverse physiological and pathological systems, a major function of CD147 is to stimulate production of a set of MMPs, some of which are shed into the extracellular space. Thus, we reasoned that MMPs that are regulated/induced by CD147 might modulate extracellular Aβ levels. To address this possibility, we generated stable HEK293 cells overexpressing CD147 and observed a small decrease in Aβ in the conditioned medium compared with that of parental HEK293 cells (Fig. 6*A*). As we had predicted based on siRNA studies, overexpression of CD147 had no effect on the levels of AICD or NICD production in cells transfected with APP695-6Myc or mNotchΔE, respectively (Fig. 6, *B* and *C*).

To investigate whether the observed decrease in extracellular levels of Aβ is mediated through CD147 induction of MMPs that are known to be capable of degrading Aβ (29, 33–36), we examined the stability of synthetic $Aβ_{40}$ and $Aβ_{42}$ peptides in the conditioned medium of HEK293 cells transfected with an empty vector or stable CD147 cells. For this assay, we incubated aliquots of conditioned medium (containing undetectable levels of endogenous Aβ) with 50 ng of synthetic $Aβ_{40}$ peptides at 37 °C overnight and performed Western blotting to detect synthetic $Aβ_{40}$ remaining in the reaction. Surprisingly, there was considerable loss of synthetic Aβ in the reactions containing culture medium from CD147-overexpressing cells compared with HEK293 cells (Fig. 7*B*). After 14 h of incubation *in vitro*, the medium conditioned by CD147-overexpressing cells degraded significantly higher levels of input Aβ (nearly 90 and 70% of input $Aβ_{40}$ and $Aβ_{42}$, respectively, by the medium of CD147 cells *versus* 60 and 50% of input $Aβ_{40}$ and $Aβ_{42}$ by the medium of naïve HEK293 cells). To further rule out any contribution of γ-secretase to extracellular degradation of synthetic Aβ potentiated by CD147 overexpression, we treated stable CD147 cells treated with the γ-secretase inhibitor Compound E prior to collecting the conditioned medium. *In vitro* Aβ degradation assays showed that the medium conditioned by stable CD147 cells degraded Aβ to the same degree regardless of the differences in their γ-secretase activity, *i.e.* treated or not

Downloaded from www.jbc.org at RIKEN LIB on February 16, 2009

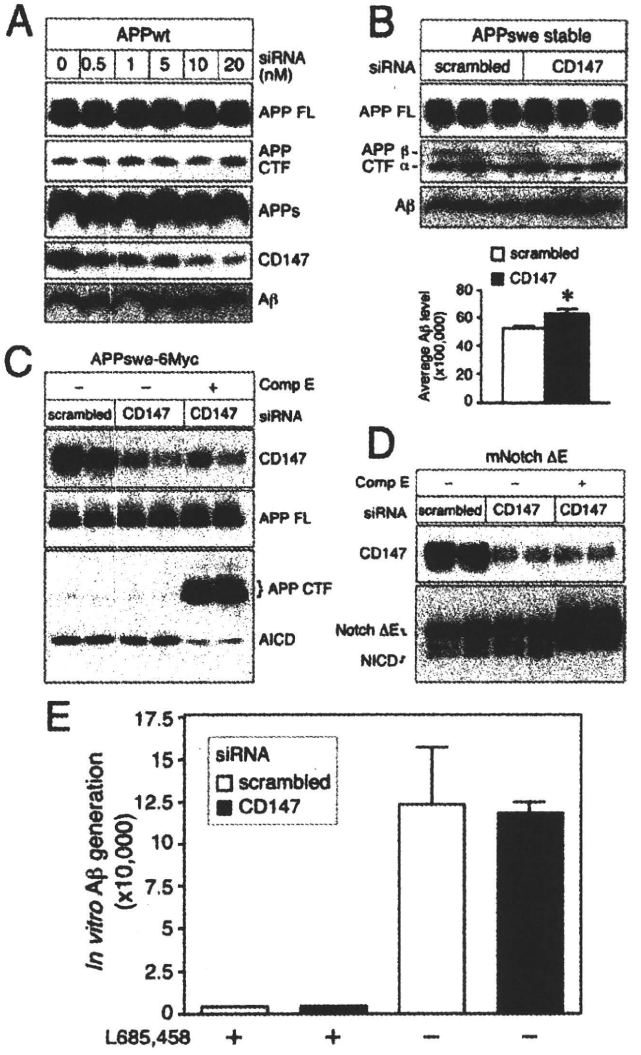

FIGURE 5. **Increase in Aβ levels associated with the depletion of CD147 is independent of APP secretase activities.** *A*, HEK293 cells were transiently transfected with increasing doses of CD147 siRNA together with WT APP695 cDNA. 50 μg of total cell lysates was analyzed by Western blotting to examine the levels of full-length (*FL*) APP, APP CTF, and CD147. The levels of secreted APP (*APPs*) and Aβ conditioned medium were analyzed by immunoblotting. *B*, HEKswe cells were transfected with scrambled or CD147 siRNA and analyzed as described above. The levels of Aβ were quantified by ELISA and plotted (mean ± S.E., $n = 3$; *, $p < 0.02$). *C*, HEK293 cells were cotransfected with either scrambled or CD147 siRNA duplex and a plasmid encoding APPswe-6Myc. Compound E (*Comp E*; 10 nM) was added as indicated to inhibit γ-secretase activity. *D*, conditions were the same as described for *C* except that cells were transfected with a plasmid encoding mNotchΔE instead of APP. *E*, membranes prepared from siRNA-treated cells were used in an *in vitro* assay to monitor γ-secretase processing of recombinant C100-FLAG substrate (14). The reactions were performed in the presence or absence of 1 μM L685,458 to establish the specificity of the assay. $Aβ_{40}$ generated by γ-secretase cleavage of the substrate was quantified by ELISA and plotted (mean ± S.E., $n = 3$).

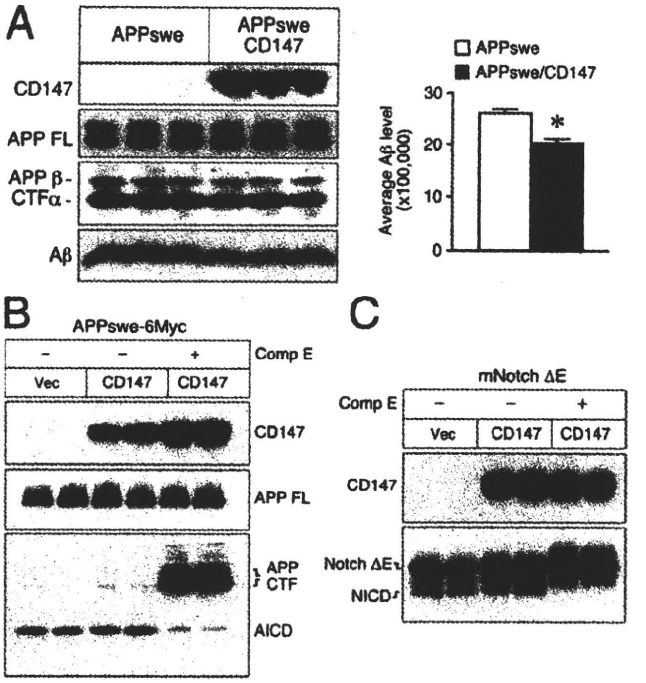

FIGURE 6. **Decrease in Aβ levels associated with CD147 overexpression is independent of APP secretase activities.** *A*, overexpression of CD147 reduces Aβ in conditioned medium. Total cell lysate and the conditioned medium from HEK293 cells stably expressing either APPswe or APPswe and Myc-tagged CD147 were used to analyze the levels of full-length (*FL*) APP and Aβ. Total Aβ levels in the conditioned medium were quantified by ELISA and plotted (mean ± S.E., $n = 3$; *, $p < 0.0005$). *B*, HEK293 cells were transiently cotransfected with an empty vector (*Vec*) or with Myc-tagged CD147 cDNA along with APPswe-6Myc. Compound E (*Comp E*; 10 nM) was added as indicated to inhibit γ-secretase activity. *C*, conditions were the same as described for *B* except that cells were transfected with a plasmid encoding mNotchΔE instead of APP. AICD and NICD experiments were repeated twice with similar results.

with Compound E (Fig. 7, *A* and *B*). Thus, CD147-mediated extracellular degradation of Aβ levels by CD147 is independent of γ-secretase activity.

A recent report has linked MMP-2 and MMP-9 to Aβ degradation (29). To examine the possibility that these two enzymes might be involved in Aβ degradation in the conditioned medium of CD147-overexpressing cells, we performed gelatin-substrate zymography (Fig. 8*A*). We failed to detect differences in the levels of MMP-2 and MMP-9 activities in the culture medium of CD147-overexpressing cells relative to that of naïve HEK293 cells. This result ruled out the contribution of these two enzymes and indicated that other protease(s) likely contribute to enhanced Aβ degradation in CD147-conditioned medium. Therefore, we mixed several metalloprotease inhibitors with the conditioned medium from CD147-overexpressing cells and then incubated these mixtures with Aβ secreted from HEKswe cells for 15 h at 37 °C (Fig. 8*B*). As a control, we used the conditioned medium from naïve HEK293 cells in the absence of inhibitors. Each of the inhibitors used in this assay showed different levels of inhibition of Aβ degradation. EDTA and 1,10-phenanthroline exhibited the highest level of inhibition, indicating metalloprotease(s) are involved in Aβ degradation. Thiorphan and Nap, a neprilysin inhibitor and an insulin-degrading enzyme inhibitor, respectively, as well as two MMP inhibitors, actinonin and GM6001, also inhibited Aβ degradation. Although these results cannot identify a single enzyme activity that is responsible for enhanced Aβ degradation in the conditioned medium of CD147-overexpressing cells, they could imply that one or more metalloproteases or MMPs are involved in this degrading activity. At present, the identity of the protease(s) in the conditioned medium of CD147-overex-

Downloaded from www.jbc.org at RIKEN LIB on February 16, 2009

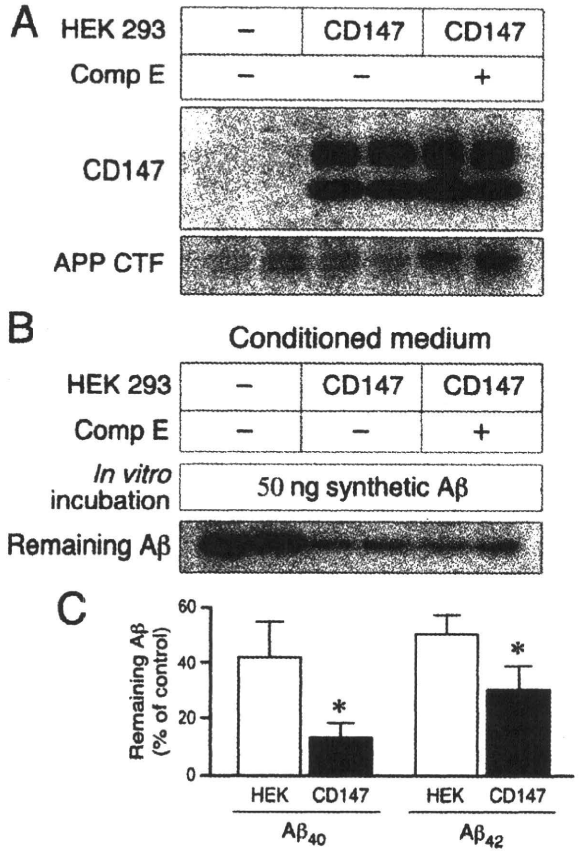

FIGURE 7. **Comparison of $A\beta_{40}$ and $A\beta_{42}$ degradation by the conditioned medium from HEK293 or HEK293 cells overexpressing CD147.** *A* and *B*, CD147 potentiation of extracellular Aβ degradation is independent of γ-secretase activity. Naïve HEK293 cells or CD147-overexpressing cells were cultured in the presence or absence of 10 nM Compound E (*Comp E*) overnight, and their conditioned media were collected. *A*, Western blots of detergent lysates show CD147 overexpression and an increase in endogenous APP CTFs by Compound E treatment. *B*, aliquots of the conditioned media were mixed with 50 ng of synthetic $A\beta_{40}$, and the mixtures were incubated at 37 °C. After a 14-h incubation, the mixtures were resolved on a Tris/Tricine gel and blotted with 26D6 to detect the remaining $A\beta_{40}$ peptides. *C*, synthetic $A\beta_{40}$ or $A\beta_{42}$ was incubated for 14 h with medium conditioned by naïve HEK293 cells or cells stably overexpressing CD147. $A\beta_{40}$ and $A\beta_{42}$ remaining intact at the end of the incubation period were quantified by Western blotting, and the percentage of Aβ remaining was calculated relative to the levels in reactions containing fresh culture medium (mean ± S.E., $n = 8$; *, $p < 0.001$).

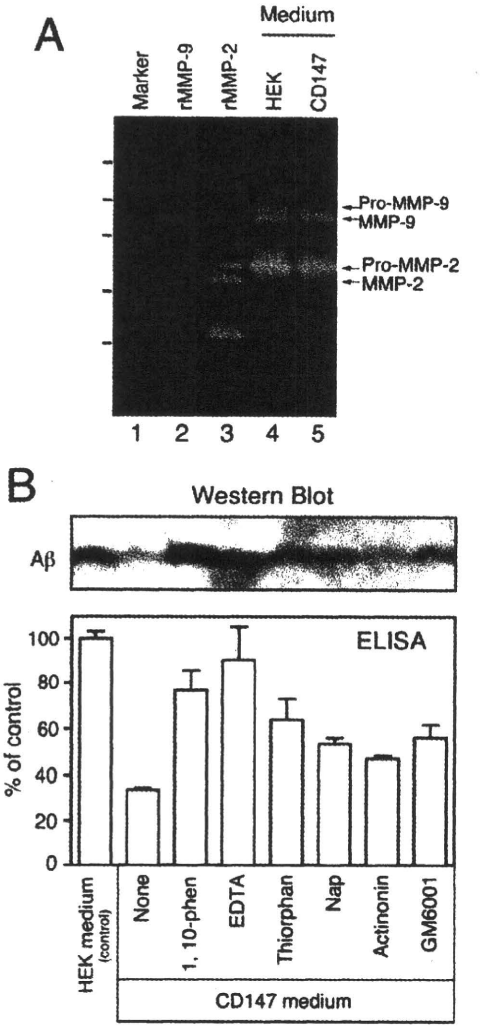

FIGURE 8. **Assays of CD147-dependent proteases that degrade Aβ in the medium.** *A*, gelatin-substrate zymography shows no difference in MMP-2 and MMP-9 activities in culture medium from CD147-overexpressing cells relative to medium conditioned by naïve HEK293 cells. *Lanes 2* and *3* contain recombinant MMP-9 and MMP-2, respectively. *B*, conditioned medium from CD147-overexpressing cells was incubated with secreted Aβ (medium from HEKswe cells) as described under "Experimental Procedures" in the presence or absence of different protease inhibitors. The conditioned medium from naïve HEK293 cells was used as a control in the absence of protease inhibitor. The levels of remaining Aβ were either visualized by Western blotting or quantified by ELISA and plotted. Note that for unknown reason, the levels of Aβ in medium containing 1,10-phenanthroline (*1,10-phen*) were consistently underestimated by ELISA. These experiments were repeated three times.

pressing cells is elusive, but it remains an active subject of investigation.

DISCUSSION

CD147 was previously identified as a protein associated with γ-secretase complex in detergent-solubilized HeLa cell membranes (16). These earlier studies revealed that siRNA knockdown of CD147 caused a dose-dependent increase in secreted Aβ levels. Remarkably, the mechanism(s) by which CD147 expression modulated extracellular Aβ levels were not determined at the time of publication, and information has not emerged in the interim in this regard. In this study, we have provided a detailed examination of the potential regulatory role of CD147 in the γ-secretase complex and now offer several novel insights. First, we have provided several lines of *in vitro* and *in vivo* evidence to suggest that CD147 expression, stability, and localization are regulated independently of the core subunits of γ-secretase. Furthermore, we failed to observe a detectable interaction between CD147 and γ-secretase complex subunits using a co-immunoprecipitation condition widely used by several groups to immunoaffinity purify the active γ-secretase complex (for example, see Ref. 14). Second, although we confirmed that depletion of CD147 in a human cell line modulates extracellular Aβ levels similarly as reported previously in Chinese hamster ovary cells (16), we failed to demonstrate that CD147 modulates Aβ production in an *in vitro* γ-secretase reconstitution assay. Moreover, we have shown that overexpression or depletion of CD147 expression failed to affect AICD

Downloaded from www.jbc.org at RIKEN LIB on February 16, 2009

or NICD generation in transfected cells. Thus, we have formally ruled out direct modulation of γ-secretase by CD147. Third, we have reported that medium conditioned by cells overexpressing CD147 had higher levels of Aβ-degrading activities, indicating that the function of CD147 in modulating MMPs may be responsible for the elevated degradation of extracellular Aβ. Collectively, these results suggest that the dose-dependent increase of Aβ in the conditioned medium of CD147-depleted cells observed in both our studies and the previous report (16) is mediated through CD147-dependent Aβ-degrading MMPs in the culture medium rather than direct modulation of γ-secretase activity, as was proposed previously.

In agreement with the data presented in the previous report by Zhou *et al.* (16), we found that depletion of CD147 in cultured HEK293 cells led to an increase in the steady-state levels of Aβ in the conditioned medium, but without discernible changes in the levels of CTFs derived from α- and β-secretase processing of APP. Although these findings suggested a role for CD147 in the modulation of γ-secretase processing of APP CTFs, additional studies were required to validate this notion. However, CD147 expression had no effect on the levels of AICD or NICD production in transfected cells. More important, *in vitro* γ-secretase assays performed using membranes purified from cells in which CD147 was depleted failed to show an increase in Aβ production, thus formally ruling out direct modulation of γ-secretase activity by CD147. In this regard, CD147 differs from p23/TMP21, another type I membrane protein that co-purified with γ-secretase complexes and was found to regulate γ-secretase activity (17). We recently reported that depletion of p23 elevated Aβ production in the same *in vitro* γ-secretase assay employed in the CD147 experiments described above (20). Thus, unlike the case of p23 depletion, which caused an increase in Aβ levels in both intact cells and *in vitro* assays, depletion of CD147 failed to exert any influence on Aβ production *in vitro*. This unexpected finding prompted us to explore alternative interpretations of the data that emerged from CD147 knockdown studies showing increased levels of Aβ in the conditioned medium described here and in the earlier report (16).

Many different cellular functions have been ascribed to CD147, including induction of several metalloproteases (37), cell adhesion (38), retinal cell development (39), T-cell activation (40, 41), and calcium mobilization (42). The ability of CD147 to induce multiple MMPs, including MMP-1, MMP-2, and MMP-3, has been well documented, and this is the basis of the alternative name EMMPRIN (18). Thus, we reasoned that the influence of CD147 on Aβ levels might be mediated through an indirect mechanism involving extracellular MMPs that degrade Aβ in the cultured medium. Indeed, studies that directly assessed the stability of synthetic Aβ peptides demonstrated enhanced Aβ degradation when incubated with medium conditioned by cells overexpressing CD147. Incubation of CD147 cells with Compound E, a potent γ-secretase inhibitor, did not have any discernible effect on the Aβ-degrading activity in the conditioned medium, formally ruling out any connection between γ-secretase activity and CD147-mediated Aβ-degrading activity (Fig. 7). Inhibitory profiles from EDTA and 1,10-phenanthroline strongly suggest the involvement of metalloprotease, whereas partial inhibition of Aβ degradation by GM6001 and actinonin might indicate that more than one MMP is involved in the degradation.

Studies by independent groups previously demonstrated that subunits of the γ-secretase complex cooperatively mature and traffic through the secretory pathway; incomplete assemblies are incapable of exiting the ER and are eventually degraded (reviewed in Ref. 11). In contrast to the well established codependent stability of the core γ-secretase subunits, we have shown that the stability or subcellular localization of CD147 in the Golgi and plasma membrane was unaffected in cells lacking either PS1/PS2 or nicastrin expression. It is also evident from our studies that the postnatal developmental expression profile of CD147 in mouse brain markedly differs from those of PS1 and nicastrin. Furthermore, unlike the overlapping neuronal distribution observed for nicastrin and PS1 in all major areas of adult rat brain (28), we found non-overlapping cellular distributions of CD147 and nicastrin in neurons within the cortex and hippocampus (Fig. 4*D*). Based on these data alone, it is implausible that all γ-secretase complexes in these neurons are bound to CD147 or subject to CD147 modulation. Nevertheless, our results cannot exclude the possibility that CD147 localized largely at the cell surface/neuronal processes modulates a small subset of active γ-secretase localized in these neuronal compartments.

How can we reconcile with the apparently discrepant data that CD147 co-purifies with the γ-secretase complex, but is not involved in the regulation of its enzyme activity? Both CD147 and the γ-secretase complex localize to cholesterol- and sphingolipid-enriched membrane microdomains, raising the possibility that co-purification in certain detergents might not necessarily represent *bona fide* protein-protein interaction, but rather co-isolation of several proteins that are tightly packed in membrane rafts. In this regard, CD147 interacts with caveolin-1 in a cholesterol-dependent manner and has been shown to be a potent modulator of lipid rafts in T-lymphocytes (43, 44). Nonetheless, we have demonstrated that membrane raft distribution of CD147 and γ-secretase occurs independently of one another, ruling out a role for CD147 in lipid raft targeting of the γ-secretase complex.

Despite the strengths of our findings, it remains plausible that transient interactions between distinct subcellular populations of CD147 and γ-secretase may be of physiological relevance. In this regard, the interaction of nicastrin and Rer1p, a transmembrane protein that is located primarily in the *cis*-Golgi and functions in the retrieval of a variety of ER membrane proteins lacking KK*XX* or KDEL signals, has recently been demonstrated (45). Similarly, it remains to be determined whether CD147, localized primarily at the cell surface, is involved only in the targeting to or retention of a very small pool of γ-secretase complexes at the cell surface in a manner not dissimilar from the reported CD147-dependent trafficking of the monocarboxylate transporters MCT1 and MCT4 to the cell surface (32). In any event, although the significance of the potential CD147·γ-secretase complex interaction is not yet apparent, our data unambiguously demonstrate that CD147 regulates secreted Aβ levels by mediating proteolytic degradation in the extracellular milieu. Further studies to identify and

Downloaded from www.jbc.org at RIKEN LIB on February 16, 2009

characterize the protease(s) responsible for CD147-dependent extracellular turnover of Aβ are critical and may provide the foundation for novel therapeutic targets focused on enhancing Aβ degradation.

Acknowledgments—We thank Drs. Wim Annaert and Bart De Strooper (Katholieke Universiteit Leuven and Flanders Interuniversity Institute for Biotechnology, Belgium) for the gift of PS1$^{-/-}$/PS2$^{-/-}$ MEFs and Drs. Tong Li and Philip C. Wong (The Johns Hopkins University School of Medicine, Baltimore) for the gift of NCT$^{-/-}$ and APH1ab$^{-/-}$ MEFs. We thank Dr. Toshio Kitamura (University of Tokyo) for providing retroviral vector and packaging cells. We thank M. Sekiguchi and K. Watanabe for technical assistance.

REFERENCES

1. Vassar, R. (2004) *J. Mol. Neurosci.* **23,** 105–114
2. Iwatsubo, T. (2004) *Curr. Opin. Neurobiol.* **14,** 379–383
3. Wolfe, M. S., Xia, W., Ostaszewski, B. L., Diehl, T. S., Kimberly, W. T., and Selkoe, D. J. (1999) *Nature* **398,** 513–517
4. Li, Y.-M., Xu, M., Lai, M. T., Huang, Q., Castro, J. L., DiMuzio-Mower, J., Harrison, T., Lellis, C., Nadin, A., Neduvelil, J. G., Register, R. B., Sardana, M. K., Shearman, M. S., Smith, A. L., Shi, X. P., Yin, K. C., Shafer, J. A., and Gardell, S. J. (2000) *Nature* **405,** 689–694
5. Shah, S., Lee, S. F., Tabuchi, K., Hao, Y. H., Yu, C., LaPlant, Q., Ball, H., Dann, C. E., III, Sudhof, T., and Yu, G. (2005) *Cell* **122,** 435–447
6. Edbauer, D., Winkler, E., Regula, J. T., Pesold, B., Steiner, H., and Haass, C. (2003) *Nat. Cell Biol.* **5,** 486–488
7. De Strooper, B., Saftig, P., Craessaerts, K., Vanderstichele, H., Guhde, G., Annaert, W., Von Figura, K., and Van Leuven, F. (1998) *Nature* **391,** 387–390
8. Li, T., Ma, G., Cai, H., Price, D. L., and Wong, P. C. (2003) *J. Neurosci.* **23,** 3272–3277
9. Ma, G., Li, T., Price, D. L., and Wong, P. C. (2005) *J. Neurosci.* **25,** 192–198
10. Takasugi, N., Tomita, T., Hayashi, I., Tsuruoka, M., Niimura, M., Takahashi, Y., Thinakaran, G., and Iwatsubo, T. (2003) *Nature* **422,** 438–441
11. Vetrivel, K. S., Zhang, Y. W., Xu, H., and Thinakaran, G. (2006) *Mol. Neurodegener.* **1, 4**
12. Leem, J. Y., Vijayan, S., Han, P., Cai, D., Machura, M., Lopes, K. O., Veselits, M. L., Xu, H., and Thinakaran, G. (2002) *J. Biol. Chem.* **277,** 19236–19240
13. Kimberly, W. T., LaVoie, M. J., Ostaszewski, B. L., Ye, W., Wolfe, M. S., and Selkoe, D. J. (2003) *Proc. Natl. Acad. Sci. U. S. A.* **100,** 6382–6387
14. Li, Y.-M., Lai, M. T., Xu, M., Huang, Q., DiMuzio-Mower, J., Sardana, M. K., Shi, X. P., Yin, K. C., Shafer, J. A., and Gardell, S. J. (2000) *Proc. Natl. Acad. Sci. U. S. A.* **97,** 6138–6143
15. Sato, T., Diehl, T. S., Narayanan, S., Funamoto, S., Ihara, Y., De Strooper, B., Steiner, H., Haass, C., and Wolfe, M. S. (2007) *J. Biol. Chem.* **282,** 33985–33993
16. Zhou, S., Zhou, H., Walian, P. J., and Jap, B. K. (2005) *Proc. Natl. Acad. Sci. U. S. A.* **102,** 7499–7504
17. Chen, F., Hasegawa, H., Schmitt-Ulms, G., Kawarai, T., Bohm, C., Katayama, T., Gu, Y., Sanjo, N., Glista, M., Rogaeva, E., Wakutani, Y., Pardossi-Piquard, R., Ruan, X., Tandon, A., Checler, F., Marambaud, P., Hansen, K., Westaway, D., St. George-Hyslop, P., and Fraser, P. (2006) *Nature* **440,** 1208–1212
18. Gabison, E. E., Hoang-Xuan, T., Mauviel, A., and Menashi, S. (2005) *Biochimie (Paris)* **87,** 361–368
19. Jenne, N., Frey, K., Brugger, B., and Wieland, F. T. (2002) *J. Biol. Chem.* **277,** 46504–46511
20. Vetrivel, K. S., Gong, P., Bowen, J. W., Cheng, H., Chen, Y., Carter, M., Nguyen, P. D., Placanica, L., Wieland, F. T., Li, Y.-M., Kounnas, M. Z., and Thinakaran, G. (2007) *Mol. Neurodegener.* **2, 4**
21. Wang, J., Brunkan, A. L., Hecimovic, S., Walker, E., and Goate, A. (2004) *Neurobiol. Dis.* **15,** 654–666
22. Kim, S. H., Ikeuchi, T., Yu, C., and Sisodia, S. S. (2003) *J. Biol. Chem.* **278,** 33992–34002
23. Onishi, M., Kinoshita, S., Morikawa, Y., Shibuya, A., Phillips, J., Lanier, L. L., Gorman, D. M., Nolan, G. P., Miyajima, A., and Kitamura, T. (1996) *Exp. Hematol.* **24,** 324–329
24. Zhang, Y. W., Luo, W. J., Wang, H., Lin, P., Vetrivel, K. S., Liao, F., Li, F., Wong, P. C., Farquhar, M. G., Thinakaran, G., and Xu, H. (2005) *J. Biol. Chem.* **280,** 17020–17026
25. Thinakaran, G., Borchelt, D. R., Lee, M. K., Slunt, H. H., Spitzer, L., Kim, G., Ratovitsky, T., Davenport, F., Nordstedt, C., Seeger, M., Hardy, J., Levey, A. I., Gandy, S. E., Jenkins, N. A., Copeland, N. G., Price, D. L., and Sisodia, S. S. (1996) *Neuron* **17,** 181–190
26. Vetrivel, K. S., Cheng, H., Kim, S. H., Chen, Y., Barnes, N. Y., Parent, A. T., Sisodia, S. S., and Thinakaran, G. (2005) *J. Biol. Chem.* **280,** 25892–25900
27. Vetrivel, K. S., Cheng, H., Lin, W., Sakurai, T., Li, T., Nukina, N., Wong, P. C., Xu, H., and Thinakaran, G. (2004) *J. Biol. Chem.* **279,** 44945–44954
28. Kodam, A., Vetrivel, K. S., Thinakaran, G., and Kar, S. (2008) *Neurobiol. Aging* **29,** 724–738
29. Yin, K.-J., Cirrito, J. R., Yan, P., Hu, X., Xiao, Q., Pan, X., Bateman, R., Song, H., Hsu, F. F., Turk, J., Xu, J., Hsu, C. Y., Mills, J. C., Holtzman, D. M., and Lee, J.-M. (2006) *J. Neurosci.* **26,** 10939–10948
30. Tang, W., Chang, S. B., and Hemler, M. E. (2004) *Mol. Biol. Cell* **15,** 4043–4050
31. Cheng, H., Vetrivel, K. S., Gong, P., Meckler, X., Parent, A., and Thinakaran, G. (2007) *Nat. Clin. Pract. Neurol.* **3,** 374–382
32. Wilson, M. C., Meredith, D., and Halestrap, A. P. (2002) *J. Biol. Chem.* **277,** 3666–3672
33. Backstrom, J. R., Lim, G. P., Cullen, M. J., and Tokes, Z. A. (1996) *J. Neurosci.* **16,** 7910–7919
34. Iwata, N., Higuchi, M., and Saido, T. C. (2005) *Pharmacol. Ther.* **108,** 129–148
35. White, A. R., Du, T., Laughton, K. M., Volitakis, I., Sharples, R. A., Xilinas, M. E., Hoke, D. E., Holsinger, R. M., Evin, G., Cherny, R. A., Hill, A. F., Barnham, K. J., Li, Q. X., Bush, A. I., and Masters, C. L. (2006) *J. Biol. Chem.* **281,** 17670–17680
36. Yan, P., Hu, X., Song, H., Yin, K., Bateman, R. J., Cirrito, J. R., Xiao, Q., Hsu, F. F., Turk, J. W., Xu, J., Hsu, C. Y., Holtzman, D. M., and Lee, J.-M. (2006) *J. Biol. Chem.* **281,** 24566–24574
37. Sameshima, T., Nabeshima, K., Toole, B. P., Yokogami, K., Okada, Y., Goya, T., Koono, M., and Wakisaka, S. (2000) *Int. J. Cancer* **88,** 21–27
38. Cho, J. Y., Fox, D. A., Horejsi, V., Sagawa, K., Skubitz, K. M., Katz, D. R., and Chain, B. (2001) *Blood* **98,** 374–382
39. Yoshimoto, M., Sagara, H., Masuda, K., and Hirosawa, K. (1998) *Exp. Eye Res.* **67,** 331–340
40. Kasinrerk, W., Fiebiger, E., Stefanova, I., Baumruker, T., Knapp, W., and Stockinger, H. (1992) *J. Immunol.* **149,** 847–854
41. Koch, C., Staffler, G., Huttinger, R., Hilgert, I., Prager, E., Cerny, J., Steinlein, P., Majdic, O., Horejsi, V., and Stockinger, H. (1999) *Int. Immunol.* **11,** 777–786
42. Huang, Y., Jiang, J., Dou, K., and Chen, Z. (2005) *Eur. J. Cell Biol.* **84,** 59–73
43. Tang, W., and Hemler, M. E. (2004) *J. Biol. Chem.* **279,** 11112–11118
44. Staffler, G., Szekeres, A., Schutz, G. J., Saemann, M. D., Prager, E., Zeyda, M., Drbal, K., Zlabinger, G. J., Stulnig, T. M., and Stockinger, H. (2003) *J. Immunol.* **171,** 1707–1714
45. Spasic, D., Raemaekers, T., Dillen, K., Declerck, I., Baert, V., Serneels, L., Fullekrug, J., and Annaert, W. (2007) *J. Cell Biol.* **176,** 629–640

Downloaded from www.jbc.org at RIKEN LIB on February 16, 2009

Human Molecular Genetics, 2009, Vol. 18, No. 6 **1099–1109**
doi:10.1093/hmg/ddp006
Advance Access published on January 15, 2009

Efhc1 deficiency causes spontaneous myoclonus and increased seizure susceptibility

Toshimitsu Suzuki[1,6], Hiroyuki Miyamoto[2], Takashi Nakahari[7], Ikuyo Inoue[1], Takahiro Suemoto[3], Bin Jiang[4], Yuki Hirota[8], Shigeyoshi Itohara[5], Takaomi C. Saido[3], Tadaharu Tsumoto[4], Kazunobu Sawamoto[8], Takao K. Hensch[2], Antonio V. Delgado-Escueta[9] and Kazuhiro Yamakawa[1,*]

[1]Laboratory for Neurogenetics, [2]Laboratory for Neuronal Circuit Development, [3]Laboratory for Proteolytic Neuroscience, [4]Tsumoto Research Unit, [5]Laboratory for Behavioral Genetics and [6]Special Postdoctoral Researchers Program, RIKEN Brain Science Institute (BSI), 2-1 Hirosawa, Wako-shi, 351-0198 Saitama, Japan, [7]Department of Physiology, Osaka Medical College, Osaka 569-8686, Japan, [8]Department of Developmental and Regenerative Biology, Institute of Molecular Medicine, Nagoya City University Graduate School of Medical Sciences, Nagoya 467-8601, Japan and [9]Epilepsy Genetics/Genomics Laboratories, Comprehensive Epilepsy Program, UCLA Geffen School of Medicine and VA GLAHS-West Los Angeles, Los Angeles, CA 90073, USA

Received November 6, 2008; Revised and Accepted December 23, 2008

Mutations in *EFHC1* gene have been previously reported in patients with epilepsies, including those with juvenile myoclonic epilepsy. Myoclonin1, also known as mRib72-1, is encoded by the mouse *Efhc1* gene. Myoclonin1 is dominantly expressed in embryonic choroid plexus, post-natal ependymal cilia, tracheal cilia and sperm flagella. In this study, we generated viable *Efhc1*-deficient mice. Most of the mice were normal in outward appearance, and both sexes were found to be fertile. However, the ventricles of the brains were significantly enlarged in the null mutants, but not in the heterozygotes. Although the ciliary structure was found intact, the ciliary beating frequency was significantly reduced in null mutants. In adult stages, both the heterozygous and null mutants developed frequent spontaneous myoclonus. Furthermore, the threshold of seizures induced by pentylenetetrazol was significantly reduced in both heterozygous and null mutants. These observations seem to further suggest that decrease or loss of function of myoclonin1 may be the molecular basis for epilepsies caused by *EFHC1* mutations.

INTRODUCTION

Juvenile myoclonic epilepsy (JME) is a common adolescent onset myoclonic, clonic-tonic-clonic (grand mal) generalized epilepsy (IGE) that is responsible for 3–12% of all known epilepsies (1–3). Electroencephalography (EEG) reveals 15–30 Hz multispikes during myoclonic and tonic-clonic convulsions. Moreover, 3.5–6 Hz multispikes and wave complexes appear in 17% of clinically asymptomatic members of JME families (1). We previously identified mutations in the *EFHC1* (EF-hand domain containing 1) gene that segregated with epilepsy and the appearance of EEG polyspike wave in patients of JME families (4). The human *EFHC1* encodes a 640 amino acid non-ion channel protein myoclonin1 that harbors three tandemly repeated DM10 domains, a motif of unknown function and one EF-hand calcium-binding motif at the C terminus. *EFHC1* mRNA was observed in multiple tissues, including the brain in northern blot analyses (4). We also previously reported along with another group that mouse myoclonin1 protein was dominantly expressed in choroid plexus at restricted developmental stages in the fetus and in the cilia of ependymal cells lining the wall of ventricles, tracheal cilia and sperm flagella at post-natal stages (5,6).

Successive studies by other groups have confirmed our findings by reporting a single *EFHC1* heterozygous missense mutation in one of 54 JME Caucasian families (7) and two missense mutations in two of 27 Italian JME families (8).

*To whom correspondence should be addressed. Tel: +81 484679703; Fax: +81 484677095; Email: yamakawa@brain.riken.jp

© *The Author 2009. Published by Oxford University Press. All rights reserved.*
For Permissions, please email: journals.permissions@oxfordjournals.org

In addition to the mutations in JME, Stogmann *et al.* (9) previously described *EFHC1* mutations in other types of idiopathic epilepsies: three missense mutations in four patients with juvenile absence epilepsy, cryptogenic temporal lobe epilepsy (cTLE) and an unclassified IGE of 61 IGE (including 24 JME) and 372 TLE patients.

In addition to the original full-length myoclonin1, the *EFHC1* gene also encodes a short isoform of myoclonin1 (278 amino acids) that harbors only one DM10 domain without an EF-hand motif and a unique C-terminal end (4). We recently identified heterozygous frameshift and nonsense mutations in the part of *EFHC1* transcript encoding the unique C-terminal end of the myoclonin1 short isoform in three JME families (two families from Honduras and one from Mexico) as well as identified new missense mutations in the original long isoform of *EFHC1* in two JME families (from Mexico and Japan) (10).

Although the results of these familial studies have indicated that *EFHC1* mutations may be genetically responsible for the observed epilepsies, direct physiological or biological evidence have been rather scarce to date. To further address the putative relevance of *EFHC1* in epilepsies, we generated and characterized *Efhc1*-deficient mice. We found that disruption of *Efhc1* in mice caused frequent spontaneous myoclonus and enhanced seizure susceptibility to chemoconvulsant stimulation. Our findings further support the contention that *EFHC1* is a gene responsible for some forms of epilepsies.

RESULTS

Generation of *Efhc1*-deficient mouse

We constructed a targeting vector in which a phosphoglycerate kinase-promoted neomycin resistance gene cassette was inserted into exon 1 of the *Efhc1* gene (Fig. 1A). This caused a frameshift at amino acid position 14 of myoclonin1 and introduced a premature stop codon six amino acids further down from the frameshift. This frameshift effectively eliminated most of the *Efhc1* coding sequence, rendering it non-functional. Genotypes of targeted embryonic stem (ES) clones were verified by Southern blot analysis and polymerase chain reaction (PCR) (Fig. 1B and C). Mice carrying the targeted allele were derived from two independent ES clones and showed identical phenotypes. *Efhc1* homozygous mutant (null) and heterozygous offspring were viable and were produced in the expected Mendelian genotype ratio (~25 and ~50%, respectively). Reverse-transcriptase–PCR (RT–PCR) analyses of RNAs extracted from the brain, kidney and liver tissues revealed no *Efhc1* mRNA in the null mutants (Fig. 1D). Genotypes of the mice were determined by PCR using genomic DNA isolated from the tail (Fig. 1E). We previously reported the absence of myoclonin1 protein in the null mutants by western blot and immunohistochemical analyses using an anti-myoclonin1 monoclonal antibody (6A3-mAb) (5). Heterozygous and null mutants were fertile in both sexes and showed mostly normal growth with no gross abnormalities in their outward appearance. Although myoclonin1 is dominantly expressed in the sperm flagella and oviduct (6), the observed preserved fertility of the null mutant male and female mice suggests that the absence of myoclonin1 in the sperm flagellum and oviductal cilia does not adversely affect the motility and function of these structures.

Increased spontaneous myoclonus in both heterozygous and null *Efhc1*-deficient mice

The *Efhc1* mutant mice developed spontaneous recurrent involuntary movement of the whole body (muscular jerks) at 7–8 months of age (Fig. 2 and Supplementary Material, Video S1). Each episode of the jerks lasted for less than ~200 ms and usually consisted of one to three jerks with brief electromyographic bursts (positive myoclonus), with the mice immediately returning back to normal behavior after each of the episodes. Movements without electromyographic bursts were assumed to be voluntary ones and were not included in the count. The frequency of myoclonus was seven to eight times higher in the heterozygous and null mutants compared with the background level of wild-type littermates (Fig. 2B). These involuntary twitches and jerks (myoclonus) synchronously involved the whole body, simultaneously activating the upper body in the shoulders and head bilaterally, often propelling the mice backwards. These semiologies suggest an afferent volley outside the cerebral cortex and a pontobulbospinal activation. Jerks were observed during both the sleep and wake phases. A blind observer to the genotype readily detected these twitches by electromyogram (EMG). By using bilaterally implanted somatosensory cortex parietal electrodes, we monitored the electrocorticograms (EcoGs) in freely moving 7–8-month-old mice. We did not observe prominent abnormal EEG activity in the null or heterozygous mutants in each single measurement of myoclonus. However, the polygraphic analysis revealed that the back-averaging of evoked potentials in the EcoG recordings gave positive signals when triggered to involuntary movements (positive myoclonus) (Fig. 2C), but not when triggered to voluntary movements (Fig. 2D). These results may suggest that spontaneous myoclonus in the mutants is not cortical but may possibly be subcortical (thalamus, etc.) or perhaps brain stem in origin.

Increased seizure susceptibility to a chemoconvulsant stimulation in both heterozygous and null *Efhc1*-deficient mice

We next investigated the seizure susceptibility of the *Efhc1*-deficient mice by using chemoconvulsant, pentylenetetrazole (PTZ). PTZ, a gamma-aminobutyric acid (GABA) receptor α1 subunit antagonist, is one of the most commonly used pharmacological agents for inducing seizures (11). After intraperitoneal (i.p.) application of 50 mg/kg body weight of PTZ in 4–5-month and 9–12-month-old mice, a much larger number of the heterozygous and null mutant mice showed generalized convulsive seizures (GS) when compared with wild-type mice (Fig. 3). The latency until the onset of seizures was also significantly decreased in both the heterozygous and null mutants. We then further evaluated myoclonic jerks (MJs) and clonic seizures (CLs) (Supplementary Material, Fig. S1 and Fig. 3). Although MJs did not show significant differences among genotypes, more frequent CL with shorter latency was observed in both the mutants. When observed at

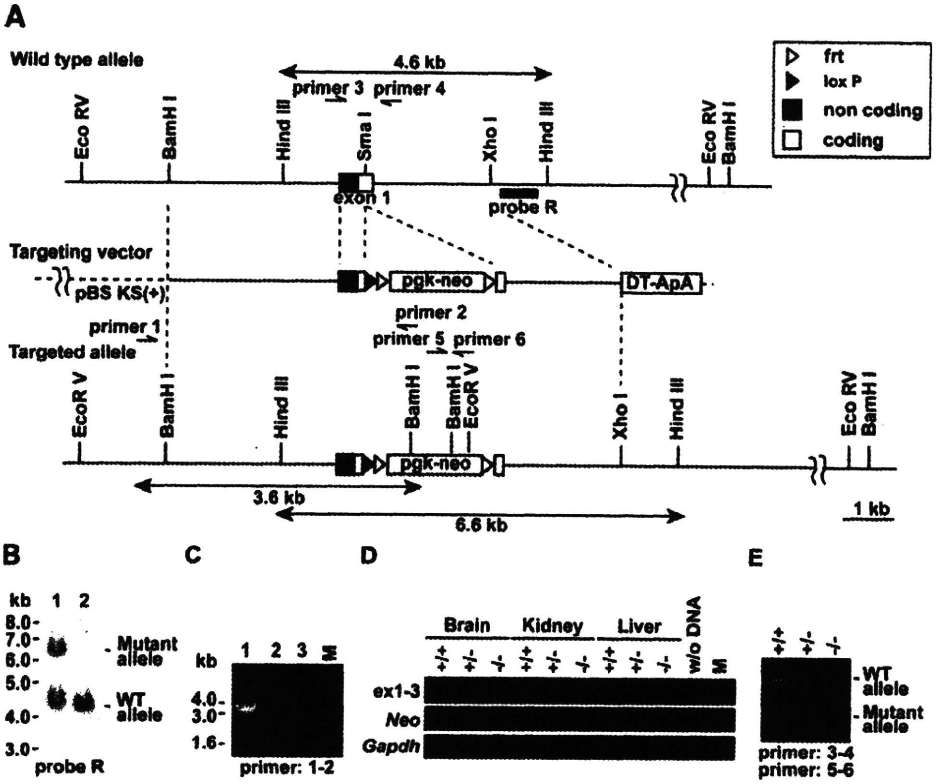

Figure 1. Generation of *Efhc1*-deficient mice. (**A**) Schematic diagram of *Efhc1* genomic sequence (top), targeting construct (middle) and targeted *Efhc1* allele (bottom). The coding (white box) and non-coding (blackened box) regions of exon 1 are shown. Relative position of the 3′ external probe (probe R) used to detect the targeted allele is shown under the wild-type allele. The predicted size of the wild-type (4.6 kb) and targeted (6.6 kb) alleles that probe R would detect in *Hin*dIII digests is shown. (**B**) Southern blot analysis of *Hin*dIII-digested genomic DNA from mouse ES cells. Probe R identified expected size fragments of wild-type and targeted mutant alleles. Lane 1 is targeted ES cell and lane 2 is wild-type ES cell. (**C**) Homologous recombination of left arm was confirmed by PCR. The PCR analysis, performed on genomic DNA derived from ES cells, resulted in the amplification of the expected size fragment in the homologous recombinant ES cell (lane 1), but not in the wild-type sample (lane 2). Lane 3 refers to the reaction without a template. (**D**) RT–PCR analysis for *Efhc1* mRNA expression in mutant mice. Primers on *Efhc1* cDNA (exon-connection PCR primer pair exon 1F/exon 3R) or on *pgk-neo* (Neo) cDNA (primer pair primer 5/primer 6) were designed to amplify 462 bp fragment from the *Efhc1* cDNA or 152 bp fragment from the *Neo* cDNA. The RT–PCR analysis, performed on cDNAs derived from brain, kidney and liver total RNA, resulted in amplification of the expected size *Efhc1* exons 1–3 fragment in the wild-type (+/+) and heterozygous (+/−) but not in the homozygous null mutant (−/−) sample. Conversely, −/− and +/−, but not +/+, cDNAs were amplified by primer pair for *Neo*. Lane (w/o DNA) refers to the reaction without a template. Control amplification for the glyceraldehyde 3-phosphate dehydrogenase gene (*Gapdh*) confirms the quality of the cDNA made. (**E**) PCR genotyping of mouse tail DNA. The PCR analysis, performed on genomic DNAs derived from +/+, +/− and −/−, resulted in the amplification of the expected size fragment of wild-type allele (442 bp, upper band) in +/+ and +/− or targeted allele (152 bp, lower band) in +/− and −/−. The positions of primers are indicated in (A). M, DNA size standard.

a younger stage (2-month-old), we did not see any significant differences of seizure susceptibilities between *Efhc1* mutants and their wild-type littermates (data not shown).

Increased polysialic acid (PSA)-NCAM expression in hippocampal dentate gyri of *efhc1*-deficient mouse

Increased neurogenesis at the subgranular zone (SGZ) of the hippocampal dentate gyrus has been reported in epileptic mouse models of seizures, which are induced by chemoconvulsants or kindling (12,13). We, therefore, investigated the expression of PSA-NCAM, a marker for newly generated neurons (14), in the SGZ of 2-month-old mice without chemoconvulsant treatment. The PSA-NCAM-positive (PSA-NCAM$^+$) cells spontaneously increased in number among the heterozygous and null mutants, compared with their wild-type littermates (Fig. 4). We also performed immunohistochemistry by using anti-PSA-NCAM antibody on mouse brain sections from 2-week and 1-month-old mice. In our investigations of preliminary number of mice, we did not observe differences in the number of PSA-NCAM$^+$ cells among genotypes at these stages (data not shown). These results suggest that the increased PSA-NCAM$^+$ cell number may be induced by spontaneous seizures in the heterozygous and null mutants rather than a primary result of the *Efhc1* deficiency. Possibly, these PSA-NCAM$^+$ cells may have contributed to or further aggravated the spontaneous myoclonus and the reduction of seizure threshold in *Efhc1*-deficient mice, as previously proposed in convulsant or kindling-induced epileptic mouse models.

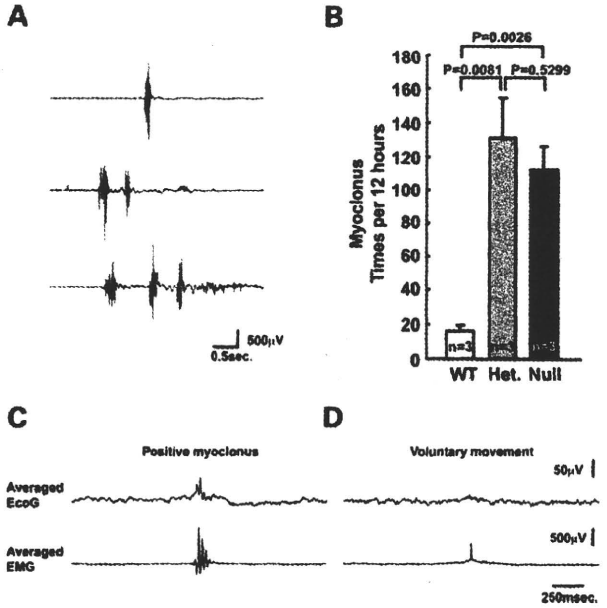

Figure 2. Increased spontaneous myoclonus in both heterozygous and null *Efhc1*-deficient mice. (**A**) Three examples of EMG recorded in null mutant mice. Quick (within 200 ms per episode) high amplitude multispikes were observed in EMG of heterozygous and null mutant mice at 7–8 months. See Supplementary Material, Video S1. (**B**) The frequency of myoclonus during 12 h in the wild-type, heterozygous and null mutant mice. The frequency of involuntary movement was seven to eight times higher in the heterozygous (131 ± 23.3 per 12 h, $P = 0.0081$) and null mutants (112.3 ± 14.1 per 12 h, $P=0.0026$), compared with the background level count of wild-type littermates (16.3 ± 3.0 per 12 h). EcoG-EMG back-averaging showed abnormal potential at spontaneous myocloni (**C**; $n = 93$) but not at voluntary movements (**D**; $n = 116$). Het, heterozygous.

Unaffected GABAergic system in *Efhc1*-deficient mouse

We also investigated functional integrities of GABA-producing interneurons in the *Efhc1* mutants. Kinetic properties of miniature inhibitory post-synaptic currents (mIPSCs) were measured from the neocortical layer II/III. Recordings were made at a holding potential of 0 mV in artificial cerebrospinal fluid (ACSF) containing tetrodotoxin. However, the mIPSCs analysis showed no differences in the amplitude, frequency, rise time or decay time in 1-month-old *Efhc1* mutants (Supplementary Material, Fig. S2). In 2-month-old mutants, increases in mIPSC frequency were observed but, again, the amplitude, rise time and decay time did not change. In keeping consistent with the results of mIPSCs, analyses of the subtype of cortical interneurons showed no differences in the numbers of parvalbumin (PV), calbindin (CB), calretinin (CR) and glutamic acid decarboxylase 67 (GAD-67) positive cells between wild-type and null mutants (Supplementary Material, Fig. S3A). The numbers of these interneurons in hippocampus were also not changed in the null mutants (data not shown). No significant changes in GAD-65/ 67 proteins in the cortex and hippocampus were noted (Supplementary Material, Fig. S3B). These results suggest that the inhibitory interneurons are mostly intact in the *Efhc1* mutants.

Enlarged brain ventricles in *Efhc1* null mutants but not in heterozygotes

Our investigations by Nissl staining of mice brain sections at 12-month-old or hematoxylin and eosin staining at post-natal day 0 (P0), P30 and 2-month-old mice revealed enlargements of ventricles in the null mutants compared with their wild-type littermates at all stages of development (Fig. 5A and B and Supplementary Material, Fig. S4A–C). The size of the hippocampus in the null mice was largely reduced, whereas the volumes of other regions were relatively conserved (ex. striatum; Supplementary Material, Fig. S4D). The ventricle enlargement was further confirmed by magnetic resonance imaging (MRI) analyses (Supplementary Material, Fig. S4E). Although enlargement of the ventricles has been reported in cases with obstruction or stricture of the aqueduct (15), the sections from the heterozygous and null *Efhc1* mutants did not show any abnormality at the aqueduct and the foramen of Monro (Fig. 5 and Supplementary Material, Fig. S4). Because of predominant expression of myoclonin1 at ependymal cilia (5), we examined the ciliary structure and measured the ciliary beat frequency (CBF) of the *Efhc1*-deficient mice. Scanning electron microscopy revealed no abnormality in the diameter and length of ependymal cilia (Fig. 6A–E). However, the CBF in the *Efhc1* null mutant mice was significantly lower when compared with the heterozygous and wild-type mice (Fig. 6F, Supplementary Material, Videos S2 and S3). This suggests that the ciliary beating defect may be the cause of ventricle enlargement in the *Efhc1* null mutant mice, as has been reported in other mice with defects of ependymal cilia (16–19).

DISCUSSION

The development of seizures and epilepsy in human JME can be categorized into three stages (20): (i) susceptibility:

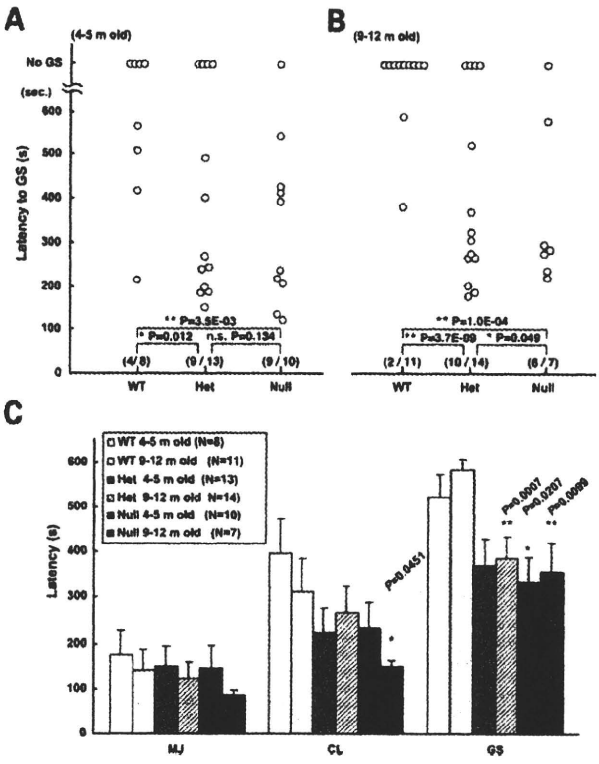

Figure 3. Increased seizure susceptibility in both heterozygous and null *Efhc1*-deficient mice. Seizure events after i.p. application of 50 mg/kg body weight of PTZ were counted. (**A** and **B**) At 4–5 months (A), percentage of animals exhibiting generalized convulsive seizures (GS) was significantly increased in heterozygous and null mutant mice. Nine of 13 (69.2%) heterozygous and 9 of 10 (90%) null mutants showed GS, whereas only 4 of 8 (50%) wild-type mice did ($n = 8–13$ per genotype). In 9–12-month-old mice (B), the percentage of animals exhibiting GS was also significantly increased in heterozygous and null mice. Ten of 14 (71.4%) heterozygous and 6 of 7 (85.7%) null mutants showed GS, whereas only 2 of 11 (18.2%) wild-type mice did ($n = 7\sim14$ per genotype). In both developmental stages, the latencies are also significantly decreased in the heterozygous and null mutants [see the histogram in (**C**)]. Open circles represent individual mice. Observation time was 600 s after drug application, and mice without GS were plotted at no GS. The numbers in round brackets indicate how many showed GS in animals tested. $^{*}P < 0.05$, $^{**}P < 0.01$. n.s., not significant. (**C**) Histogram of latencies for MJ, CL and GS in 4–5- or 9–12-month-old wild-type, heterozygous and null mutant mice with PTZ treatment ($n = 7–14$ per genotype) (see Supplementary Material, Fig. S1 for the counting of MJ and CL). For the calculation of latency periods, 600 s was temporarily assigned for the mice without seizures. In 4–5-month-old mice, the latency until onset of GS was significantly reduced in the null mutant mice (328.2 ± 53.2 s; $P = 0.0207$) compared with wild-type (512.9 ± 48.5 s). In 9–12-month-old mice, the latency until onset of GS was significantly reduced in the heterozygous (378.1 ± 45.1 s; $P = 0.0007$) and null mutant (356.4 ± 70.0 s; $P = 0.0099$) compared with wild-type (578.7 ± 20.0 s); 9–12-month-old null mice (149.6 ± 13.5 s; $P = 0.0451$) had significantly shorter latency to CL compared with wild-type (312.5 ± 70.5 s). Mean values ± SEM are shown. $^{*}P < 0.05$ and $^{**}P < 0.01$. Het, heterozygous.

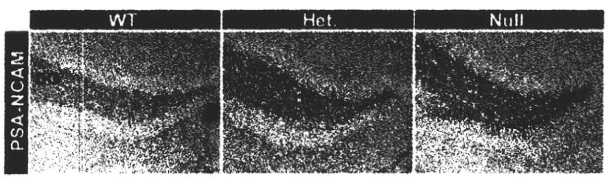

Figure 4. Increased PSA-NCAM in hippocampal dentate gyri of *Efhc1*-deficient mice. Coronal brain sections from 2-month-old mice were stained with anti-PSA-NCAM monoclonal antibody and with DAB. The expression level of PSA-NCAM in SGZ of dentate gyrus (DG) increased in the heterozygous and null mutants compared with wild-type mice. Results were reproduced in three to five mice per genotype. Het, heterozygous.

myoclonias appear mostly when triggered by fatigue, sleep deprivation, stress, menses or alcohol use. (ii) Epileptogenicity: grand mal convulsions appear 1–2 years after the first myoclonias but still need to be triggered by external stimuli. With incorrect or incomplete treatment, repeated grand mal convulsions establish the stage of epileptogenicity, in which spontaneous myoclonus and grand mal seizures start to appear. (iii) Established epileptogenesis: with more frequent spontaneous myoclonus and grand mal seizures predominating, a more enduring stage of excitability ensues and epileptogenesis is established. In this study, we found that a disruption of the *Efhc1* gene *in vivo* triggered spontaneous myoclonus and enhanced seizure susceptibility to chemoconvulsant, providing evidence that the reduction or loss of function of myoclonin1 causes epilepsy. The *Efhc1*-deficient mice are developmentally normal and fertile, but developed spontaneous myoclonus at adult stages. At 4–12 months of age, the heterozygous and null mutants showed enhanced seizure susceptibility to PTZ stimulation. Thus, *Efhc1* heterozygous and null mutant mice replicate the developmental stage dependency of susceptibility in human JME. However, a number of

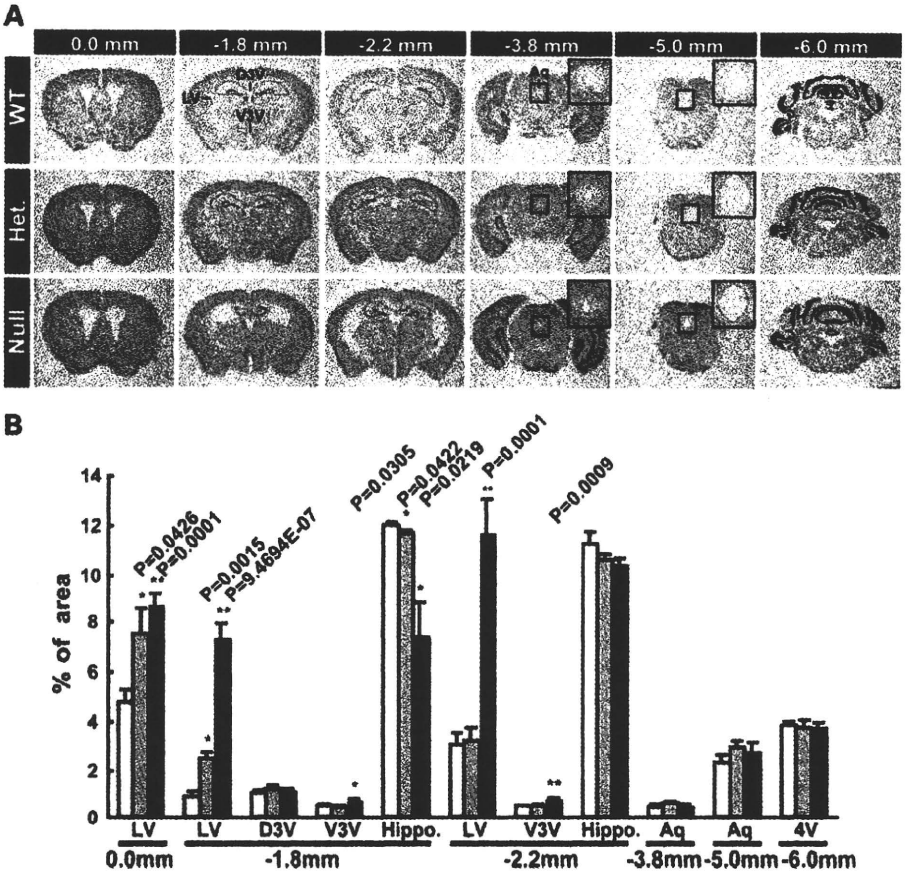

Figure 5. Enlarged brain ventricles in *Efhc1* null mutants but not in heterozygotes. (**A**) Nissl staining of serial coronal sections of brains from 12-month-old mice. Distances from bregma are shown above. Insets are higher magnifications of aqueducts. Het, heterozygous. (**B**) The sizes of the ventricle and hippocampal areas on the Nissl-stained sections were calculated by the NIH image software ($n = 3$ per genotype). Significant enlargement of lateral ventricles (LV) and decreased volume of hippocampus were observed in the null mutants compared with wild-type littermates ($P = 9.4694E-07$–0.0001 at 0.0 to -2.2 mm from bregma). The third ventricle was also significantly enlarged in the null mutants (-1.8 to -2.2 mm from bregma). Enlargement of the ventricles in the heterozygotes was very mild (LV at 0.0 and -1.8 mm) or mostly not observed (LV at -2.2 mm). The sections from heterozygous and null mice did not show noticeable abnormalities at the aqueduct and fourth ventricle (-3.8 to -6.0 mm from bregma). LV, lateral ventricle; D3V, dorsal third ventricle; V3V, ventral third ventricle; Aq, aqueduct; 4V, fourth ventricle. White bars, wild-type; grey bars, heterozygotes; blackened bars, null mutants.

different mouse epilepsy models with gene knockouts do not show spontaneous or handling-induced tonic-CL until they are >2 months of age. Therefore, at present, it would be too early to conclude that the 'stage dependence' is an *EFHC1*-specific feature. Furthermore, the mutant mice do not develop tonic-CLs, absence seizures and spike-wave complexes that have been reported in patients with JME. This may suggest that additional (environmental, genetic, or species-specific) factors contribute to the appearance of tonic-CLs and absence seizures in humans.

How does the impairment of myoclonin1 cause epilepsy? It has been proposed that the ciliary defects in patients with *EFHC1* mutations may cause abnormal CSF flow, which can lead to abnormal neural migration and result in epilepsy (21). However, in our study, ventricle enlargement possibly caused by the ciliary beating defect was minor or mostly not observed in the heterozygous *Efhc1*-deficient mouse. Still, these heterozygotes showed frequent spontaneous myoclonus and enhanced seizure susceptibility to PTZ stimulation, mostly similar to that of *Efhc1* null mutant. These observations suggest that the ventricle enlargement and the ciliary beating defect themselves may not be directly relevant to myoclonus and enhanced seizure susceptibility observed in *Efhc1*-deficient mice. In addition, the size of hippocampus in the null mutant mice was largely reduced, but this reduction in size was not observed in heterozygotes. The reduction also did not correlate with the epileptic phenotype in heterozygotes, and therefore, the hippocampal size reduction may not be directly relevant to the epileptic phenotypes. For the moment, it is still very difficult to speculate on the pathological cascade in the mice and that of *EFHC1* mutation-dependent epilepsy in patients as well. However, if any phenotypic parameters (ex. CSF secretion from choroid plexus, ion exchange at ependymal cell or pH of CSF) that are abnormal in both the heterozygous and null *Efhc1* mutants can be identified, it may indicate that one or all of those parameters are most likely the basis for the epileptic seizure phenotypes.

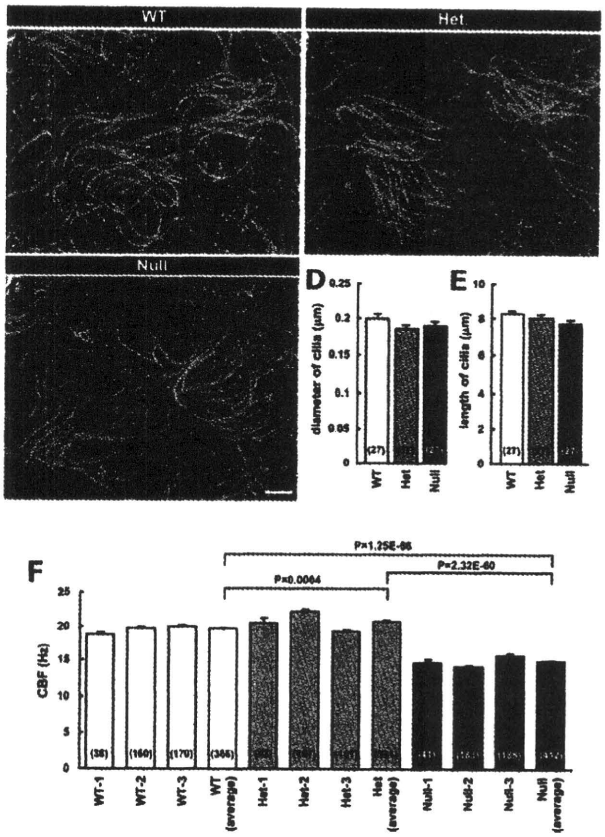

Figure 6. Unaffected morphology but affected motility of ependymal cilia in *Efhc1*-deficient mice. (**A**–**C**) Electron microscopic images of ependymal cilia on the lateral ventricle walls of the wild-type, heterozygous and null mutant mice at 3 months. No significant difference was observed in the diameter (**D**) and length (**E**) of the cilia (means ± SEM) among genotypes. Scale bar: 2 μm. (**F**) The CBF in the null mutant mice was significantly low (14.90 ± 0.21 Hz) compared with that of heterozygous (20.85 ± 0.26 Hz) and wild-type (19.80 ± 0.15 Hz). CBFs were measured in 412 cells from three null mutants, 391 cells from three heterozygous and 366 cells from three wild-type mice at 8–13 months. See Supplementary Material, Videos S2 and S3. The numbers in round brackets indicate how many cilia (D, E) and cells (F) were measured. Het, heterozygous.

We reported earlier that myoclonin1 co-localized and interacted specifically with the R-type calcium channel, $Ca_v2.3$, in neurons, and increased R-type Ca^{2+} current generated this channel (4). However, in our recent study with a newly generated anti-myoclonin1 monoclonal antibody and by using *Efhc1*-deficient mice as a negative control, we revealed that the mouse myoclonin1 protein was not observed in neuronal cells, but dominantly expressed in the embryonic choroid plexus and post-natal ependymal cilia (5). Another group reported that the myoclonin1 was localized at mitotic spindle in cultured cell lines and proposed that myoclonin1 could play an important role during cell division (22), but so far our previously mentioned anti-myoclonin1 monoclonal antibody did not detect any signals in the mitotic spindle structure (unpublished data). It is, however, still possible that the affinity of our anti-myoclonin1 monoclonal antibody may not be high enough to detect lower levels of myoclonin1 expression in the neuronal cells or at the mitotic spindle structure. Alternatively, our anti-myoclonin1 monoclonal antibody may not be able to bind to altered epitopes found in different myoclonin1 isoforms, which may possibly be expressed in neurons or the mitotic spindle. Further, careful investigation on the tissue or subcellular distribution of myoclonin1 protein is apparently required to fully elucidate the spatial expression of myoclonin1 and its various isoforms.

To date, most of genes responsible for idiopathic epilepsies have been identified (~20 genes) as ion channels (23–32). However, with the exception of sodium channel type I alpha subunit, *SCN1A*, in severe myoclonic epilepsy of Dravet (29), ion channel mutations have been unique to no more than a few of specific families. Therefore, it could be mentioned that genes responsible for most patients with idiopathic epilepsies remain unidentified. In contrast to the epileptic ion channel genes, multiple mutations of *EFHC1*, encoding the non-ion channel protein myoclonin1, have been described in multiple idiopathic epilepsies. The investigations of the molecular mechanism for epilepsies caused by *EFHC1* mutations may reveal novel pathological cascades and should greatly contribute to the understanding of epilepsy as a whole.

About 60% of the patients with JME were free from all seizure types (grand mal, myoclonic and absence seizures) during anti-epileptic drug treatment, but these seizures

continued in 40% of the patients despite drug treatment (20). Currently, there is no completely effective treatment for JME. To develop a more effective treatment for JME, additional studies are required to understand the mechanism of developing myoclonus and reducing seizure threshold by alteration of myoclonin1. Our *Efhc1*-deficient mice may enable further studies for discovery of therapeutic targets, developing a more effective treatment and perhaps eventually finding a cure for JME.

In summary, we observed frequent spontaneous myoclonus and increased seizure susceptibility in mice with *Efhc1* deficiency. These results replicate the stage of susceptibility in human JME and further support our contention that reduction or loss of function of myoclonin1 leads to enhanced susceptibility and epileptogenicity in patients with *EFHC1* mutations.

MATERIALS AND METHODS

Generation of *Efhc1*-deficient mice

All experimental protocols were approved by the Animal Experiment Committee of RIKEN Brain Science Institute. A genomic clone of the murine *Efhc1* gene was isolated from RPCI-22 129s6/SvEvTAC Taconic (F) BAC library segment 2 (BACPAC Resource Center). A 5.7 kb *Bam*HI/*Xho* I fragment including the *Efhc1* exon 1 sequence was cloned into pBluescript SK (−) (Stratagene). A neomycin selection marker, loxP-pgk-neo-loxP cassette, was inserted into *Sma* I site in *Efhc1* exon 1. A 1.1 kb MC1-DT-A cassette (a generous gift from Dr Yagi, Osaka University, Osaka, Japan), a negative selection marker, was added at the 3′-end of the targeting vector. The targeting vector linearized with *Kpn* I was electroporated into approximately 5×10^7 E14 ES cells with a Gene-Pulser (Bio-Rad Laboratories) at 3 μF and 800 V. Transfected cells were plated on neomycin-resistant, mitomycin C-treated mouse embryonic feeder (MEF) cells in 10 cm dishes. One day after plating, positive selection was performed in the presence of Geneticin (G418; 150 μg/ml). Resistant clones were picked at days 8–10 and subsequently expanded into 96-well plates pre-seeded with MEF. *Hin*dIII-digested genomic DNA from individual clones was analyzed by Southern blot, with a 956 bp probe derived from the genomic sequence immediately downstream of the targeting vector (probe-R). The probe-R was generated by PCR using primers 5′-TTCTACAAGTGTGGGTAGGAGTG-3′ and 5′-CTGCTCTGTGATGTCCGATT-3′. Positive clones were further confirmed by PCR using primers 1 (5′-GCTCAGTTCAGCCTTAAAGTTG-3′) and 2 (5′-CCACTTGTGTAGCGCCAA-3′). Homologous recombinant ES cells from each of the six targeted clones were injected into mouse C57BL/6J (B6J) blastocysts. Two ES clones (8G and 9A) produced several chimeras. Chimeric male mice were mated with B6J females to generate KO-*Efhc1*-B6J mice. The heterozygous mice were further crossbred with B6J mice four to eight times, and the resultant heterozygous mice were interbred to obtain the wild-type, heterozygous and homozygous mice. Genotypes were determined by PCR. The following PCR primers were used: primer 3 (5′-AGTTTGTTGCCAGGGTAACC-3′), primer 4 (5′-TGAGGATTCAGAAGCGGTG-3′), primer 5 (5′-TGAATGAACTGCAGGACGAGG-3′) and primer 6 (5′-AAGGTGAGATGACAGGAGATC-3′) (Fig. 1A). Primers 3 and 4 yield 442 bp fragments from the wild-type allele, and primers 5 and 6 yield 152 bp fragments from the mutant allele.

RT–PCR

Brain, kidney and liver tissues were dissected from post-natal (P) 24 days mice, and RNA was extracted and first-strand cDNA was obtained as described previously (4). To amplify mouse cDNA, we designed primers on *Efhc1* exons 1 and 3, *neomycin* and *gapdh*. Primer sequences are available upon request.

Electrocorticographic (EcoG) and EMG recordings

Recordings of EcoG and EMG were performed with 7–8-month-old wild-type, heterozygous and null mice ($n = 3$, each genotype). Stainless steel screws (1.1 mm diameter) that served as EcoG electrode were implanted over the somatosensory cortex (1.5 mm lateral to midline, 1.0 mm posterior to bregma) under 1.5% halothane anesthesia with N_2O:O_2 (3:2) ventilation in 1 week before recording. An indifferent electrode was implanted on the cerebellum (at midline, 2.0 mm posterior to lambda) as ground electrode. Two stainless steel wires (0.1 mm diameter, 1.3 mm distance) that served as bipolar-type EcoG electrode were also implanted over the somatosensory cortex. EMG electrodes were placed 2–3 mm apart from the cervical region of the trapezius muscle.

Seizure susceptibility

PTZ (Sigma) dissolved in 1 × phosphate-buffered saline (PBS) was administered i.p. at a dose of 50 mg/kg body weight in a total volume of 200–300 μl. After injection, the animals were watched closely for 10 min. The latency of until onset of twitch, repeated CL or fully generalized seizure was measured.

Histological analysis

Mice (P0 upto 12-month-old) were perfused intracardially with 4% paraformaldehyde (PFA) in 1 × PBS (pH 7.4) at 4°C. Preparations of mouse brain sections (paraffin or frozen), staining of sections (Nissl and hematoxylin-eosin) and immunohistochemical staining were carried out as described previously (5,33). The following antibodies were used: anti-PSA-NCAM antibody (1:500; Chemicon), anti-PV antibody (1:2000; Swant), anti-CB antibody (1:500; Chemicon), anti-CR antibody (1:2000; Swant) and anti-GAD-67 antibody (1:4000; Chemicon). Immunoreactivity was visualized using a Vectastain ABC kit (Vector Laboratories), developed with ImmunoPure Metal-enhanced diaminobenzidine (DAB) Substrate Kit (Pierce). Areas of the ventricles and hippocampus of Nissl-stained sections were determined using NIH image software (ImageJ).

Scanning electron microscopy

Freshly isolated brains from wild-type, heterozygous and null mice were processed for scanning electron microscopy as described previously (34). The entire lateral wall of the lateral ventricles was dissected and fixed with 2.5% glutaraldehyde/2% PFA for overnight. The tissues were incubated in 2% OsO_4 for 1 h, dehydrated with ethanol and dried with a critical point drier. After sputter coating with platinum, the mounted samples were examined with a scanning electron microscope (HITACHI S-5000).

Measurement of CBF

The brains were removed from anesthetized mice, and the surface of the lateral and fourth ventricles was cut into small pieces in HCO_3^- solution at 4°C. The HCO_3^- solution had the following composition (in millimolar): 121 NaCl, 4.5 KCl, 1 $MgCl_2$, 1.5 $NaHCO_3$, 1.5 $CaCl_2$, 1.5 NaHEPES, 5 HEPES and 5 glucose. The tissue block was cut into thin pieces by two adherent razor blades and was placed on a cover slip pre-coated with Cell-Tak (Becton–Dickinson Labware) to adhere slices firmly on the cover slip. The cover slip with slices was set in the perfusion chamber, the volume of which was 20 μl, and the rate of perfusion was 200 μl/min. The chamber was mounted on a differential interference contrast microscope (E600-FN; Nikon), which was connected to a high-speed digital video camera (FASTCAM 512PCI; Photoron). The sampling rate of the high-speed camera was 500 Hz. The CBF was calculated from the time for 10 beating cycles.

Electrophysiology

Acute brain slices were prepared from wild-type and null mice at 1 and 2 months. Briefly, the mice were decapitated, and the brain was rapidly removed from ice-cold oxygenated ACSF. Coronal slices of the somatosensory cortex (300 μm thick) were obtained using a tissue slicer (Vibratome 3000; Vibratome) in 4°C oxygenated ACSF. Slices were placed in an incubating chamber of oxygenated ACSF at 31°C for at least 1 h before recording. ACSF had the following composition (in millimolar): 124 NaCl, 3 KCl, 1.25 NaH_2PO_4, 1 $MgSO_4$, 26 $NaHCO_3$, 2 $CaCl_2$ and 10 glucose. The ACSF was bubbled continuously with 95% O_2–5% CO_2. Whole-cell voltage-clamp recordings were obtained from visually identified neurons using an infrared differential interference contrast (IR-DIC) microscopy system. Patch electrodes (3–5 MΩ) were pulled from borosilicate glass capillary tubing and fire polished. Intracellular patch pipette solution contained (in millimolar) 130 Cs-gluconate, 10 HEPES, 8 KCl, 10 Na-phosphocreatine, 3 QX314, 4 Na_2-ATP and 0.5 Na_2-GTP, pH 7.25 (285–290–mOsm). To isolate GABAergic currents, slices were perfused with ACSF containing either 20 μM 6-ciano-7-dinitroquinoxaline-2,3-dione (CNQX) or 50 μM D-(−)-2-amino-5-phosphonovaleric acid (D-AP5). Whole-cell voltage-clamp data were low-pass filtered at 1 kHz (−3 dB, eight-pole Bessel), digitally sampled at 10 kHz and monitored with Igor 4.1 software (WaveMetric Inc.). Whole-cell access resistance was carefully monitored throughout the recording, and cells were rejected if values changed by >15%; only recordings with stable series resistance of <30 MΩ were used for analysis. Each event was manually selected on the basis of rise time, amplitude and decay properties. Between 500 and 800 individual events were analyzed for each cell with the Mini Analysis program (Synaptosoft). We considered all recorded events in a single experiment for the determination of mice.

Western blot analysis

Preparations of mouse brain protein samples and western blot analyses were performed as described previously (4). The following antibodies were used: anti-GAD-65/ 67 (Biomol), 1:4000 dilution or anti-GAPDH (Santa Cruz), 1:1000 dilution. A horseradish peroxidase (HRP)-conjugated anti-mouse IgG (1:3000, Promega) or HRP-conjugated anti-rabbit IgG (1:1000, Santa Cruz) was used for secondary antibody.

High resolution MRI

Mice were anesthetized with pentobarbital and subjected to micro-MRI scans using a vertical bore 9.4 T Bruker AVANCE 400WB imaging spectrometer with a 250 mTm^{-1} actively shielded microimaging gradient insert (Bruker BioSpin) (35). A 25 mm resonator was used for signal excitation and detection. The depth of anesthesia was monitored with a breathing sensor and was maintained with 0.5–1.5% isoflurane in air. The T1-weighted MRI scans were performed with the following imaging parameters: matrix size = 256 × 256 and number of slices: 15. The T2-weighted MRI scans were performed with the following imaging parameters: matrix size = 256 × 512; TR: 3000 ms; slice thickness = 0.5 mm; number of slices: 32 and total imaging time: 100 min (four averages).

Statistical analysis

All data were expressed as mean ± SEM. The significance of differences between mean values was assessed by two-tailed Student's *t*-tests or χ^2 test, with $P < 0.05$ taken to indicate statistical significance.

SUPPLEMENTARY MATERIAL

Supplementary Material is available at *HMG* online.

ACCESSION NUMBERS

Human EFHC1 isoforms: EU520261 (long) and AY608690 (short), mouse Efhc1: EU520262 (NCBI, Entrez Nucleotide). Human myoclonin1 isoforms: ACB20691 (long) and AAT67419 (short), mouse myoclonin1: ACB20692 (NCBI, Entrez Protein).

ACKNOWLEDGEMENTS

We would like to thank Susumu Ito, Tojo Nakayama, Mika Tanaka, Chieko Nishioka, Nami Okamura and Emi Mazaki

for their helpful discussions and comments on the manuscript or technical assistance. We also thank Andrew W. Liu for his comments and for editing of the manuscript. We are indebted to the Research Resources Center of RIKEN Brain Science Institute (BSI) for DNA sequencing analysis, knockout mice production services and tissue section services.

Conflict of Interest statement. The authors declare no competing financial interest.

FUNDING

This work was supported in part by a grant from RIKEN Brain Science Institute (K.Y.), from the Ministry of Education, Culture, Sports, Science and Technology of Japan (T.S.) and from RIKEN Special Postdoctoral Researchers Program (T.S.).

REFERENCES

1. Delgado-Escueta, A.V. and Enrile-Bacsal, F. (1984) Juvenile myoclonic epilepsy of Janz. *Neurology*, **34**, 285–294.
2. Nicoletti, A., Reggio, A., Bartoloni, A., Failla, G., Sofia, V., Bartalesi, F., Roselli, M., Gamboa, H., Salazar, E., Osinaga, R. *et al.* (1999) Prevalence of epilepsy in rural Bolivia: a door-to-door survey. *Neurology*, **53**, 2064–2069.
3. Panayiotopoulos, C.P., Obeid, T. and Tahan, A.R. (1994) Juvenile myoclonic epilepsy: a 5-year prospective study. *Epilepsia*, **35**, 285–296.
4. Suzuki, T., Delgado-Escueta, A.V., Aguan, K., Alonso, M.E., Shi, J., Hara, Y., Nishida, M., Numata, T., Medina, M.T., Takeuchi, T. *et al.* (2004) Mutations in EFHC1 cause juvenile myoclonic epilepsy. *Nat. Genet.*, **36**, 842–849.
5. Suzuki, T., Inoue, I., Yamagata, T., Morita, N., Furuichi, T. and Yamakawa, K. (2008) Sequential expression of Efhc1/myoclonin1 in choroid plexus and ependymal cell cilia. *Biochem. Biophys. Res. Commun.*, **367**, 226–233.
6. Ikeda, T., Ikeda, K., Enomoto, M., Park, M.K., Hirono, M. and Kamiya, R. (2005) The mouse ortholog of EFHC1 implicated in juvenile myoclonic epilepsy is an axonemal protein widely conserved among organisms with motile cilia and flagella. *FEBS Lett.*, **579**, 819–822.
7. Ma, S., Blair, M.A., Abou-Khalil, B., Lagrange, A.H., Gurnett, C.A. and Hedera, P. (2006) Mutations in the GABRA1 and EFHC1 genes are rare in familial juvenile myoclonic epilepsy. *Epilepsy Res.*, **71**, 129–134.
8. Annesi, F., Gambardella, A., Michelucci, R., Bianchi, A., Marini, C., Canevini, M.P., Capovilla, G., Elia, M., Buti, D., Chifari, R. *et al.* (2007) Mutational analysis of EFHC1 gene in Italian families with juvenile myoclonic epilepsy. *Epilepsia*, **48**, 1686–1690.
9. Stogmann, E., Lichtner, P., Baumgartner, C., Bonelli, S., Assem-Hilger, E., Leutmezer, F., Schmied, M., Hotzy, C., Strom, T.M., Meitinger, T. *et al.* (2006) Idiopathic generalized epilepsy phenotypes associated with different EFHC1 mutations. *Neurology*, **67**, 2029–2031.
10. Medina, M.T., Suzuki, T., Alonso, M.E., Duron, R.M., Martinez-Juarez, I.E., Bailey, J.N., Bai, D., Inoue, Y., Yoshimura, I., Kaneko, S. *et al.* (2008) Novel mutations in myoclonin1/EFHC1 in sporadic and familial juvenile myoclonic epilepsy. *Neurology*, **70**, 2137–2144.
11. Huang, R.Q., Bell-Horner, C.L., Dibas, M.I., Covey, D.F., Drewe, J.A. and Dillon, G.H. (2001) Pentylenetetrazole-induced inhibition of recombinant gamma-aminobutyric acid type A (GABA(A)) receptors: mechanism and site of action. *J. Pharmacol. Exp. Ther.*, **298**, 986–995.
12. Parent, J.M., Yu, T.W., Leibowitz, R.T., Geschwind, D.H., Sloviter, R.S. and Lowenstein, D.H. (1997) Dentate granule cell neurogenesis is increased by seizures and contributes to aberrant network reorganization in the adult rat hippocampus. *J. Neurosci.*, **17**, 3727–3738.
13. Parent, J.M., Elliott, R.C., Pleasure, S.J., Barbaro, N.M. and Lowenstein, D.H. (2006) Aberrant seizure-induced neurogenesis in experimental temporal lobe epilepsy. *Ann. Neurol.*, **59**, 81–91.
14. Fanarraga, M.L., Avila, J. and Zabala, J.C. (1999) Expression of unphosphorylated class III beta-tubulin isotype in neuroepithelial cells demonstrates neuroblast commitment and differentiation. *Eur. J. Neurosci.*, **11**, 516–527.
15. Mashayekhi, F., Draper, C.E., Bannister, C.M., Pourghasem, M., Owen-Lynch, P.J. and Miyan, J.A. (2002) Deficient cortical development in the hydrocephalic Texas (H-Tx) rat: a role for CSF. *Brain*, **125**, 1859–1874.
16. Taulman, P.D., Haycraft, C.J., Balkovetz, D.F. and Yoder, B.K. (2001) Polaris, a protein involved in left–right axis patterning, localizes to basal bodies and cilia. *Mol. Biol. Cell*, **12**, 589–599.
17. Takaki, E., Fujimoto, M., Nakahari, T., Yonemura, S., Miyata, Y., Hayashida, N., Yamamoto, K., Vallee, R.B., Mikuriya, T., Sugahara, K. *et al.* (2007) Heat shock transcription factor 1 is required for maintenance of ciliary beating in mice. *J. Biol. Chem.*, **282**, 37285–37292.
18. Davis, R.E., Swiderski, R.E., Rahmouni, K., Nishimura, D.Y., Mullins, R.F., Agassandian, K., Philp, A.R., Searby, C.C., Andrews, M.P., Thompson, S. *et al.* (2007) A knockin mouse model of the Bardet–Biedl syndrome 1 M390R mutation has cilia defects, ventriculomegaly, retinopathy, and obesity. *Proc. Natl Acad. Sci. USA*, **104**, 19422–19427.
19. Lechtreck, K.F., Delmotte, P., Robinson, M.L., Sanderson, M.J. and Witman, G.B. (2008) Mutations in Hydin impair ciliary motility in mice. *J. Cell Biol.*, **180**, 633–643.
20. Martinez-Juarez, I.E., Alonso, M.E., Medina, M.T., Duron, R.M., Bailey, J.N., Lopez-Ruiz, M., Ramos-Ramirez, R., Leon, L., Pineda, G., Castroviejo, I.P. *et al.* (2006) Juvenile myoclonic epilepsy subsyndromes: family studies and long-term follow-up. *Brain*, **129**, 1269–1280.
21. King, S.M. (2006) Axonemal protofilament ribbons, DM10 domains, and the link to juvenile myoclonic epilepsy. *Cell Motil. Cytoskeleton*, **63**, 245–253.
22. de Nijs, L., Lakaye, B., Coumans, B., Leon, C., Ikeda, T., Delgado-Escueta, A.V., Grisar, T. and Chanas, G. (2006) EFHC1, a protein mutated in juvenile myoclonic epilepsy, associates with the mitotic spindle through its N-terminus. *Exp. Cell Res.*, **312**, 2872–2879.
23. Singh, N.A., Charlier, C., Stauffer, D., DuPont, B.R., Leach, R.J., Melis, R., Ronen, G.M., Bjerre, I., Quattlebaum, T., Murphy, J.V. *et al.* (1998) A novel potassium channel gene, KCNQ2, is mutated in an inherited epilepsy of newborns. *Nat. Genet.*, **18**, 25–29.
24. Charlier, C., Singh, N.A., Ryan, S.G., Lewis, T.B., Reus, B.E., Leach, R.J. and Leppert, M. (1998) A pore mutation in a novel KQT-like potassium channel gene in an idiopathic epilepsy family. *Nat. Genet.*, **18**, 53–55.
25. Wallace, R.H., Wang, D.W., Singh, R., Scheffer, I.E., George, A.L. Jr, Phillips, H.A., Saar, K., Reis, A., Johnson, E.W., Sutherland, G.R. *et al.* (1998) Febrile seizures and generalized epilepsy associated with a mutation in the Na+-channel beta1 subunit gene SCN1B. *Nat. Genet.*, **19**, 366–370.
26. Escayg, A., MacDonald, B.T., Meisler, M.H., Baulac, S., Huberfeld, G., An-Gourfinkel, I., Brice, A., LeGuern, E., Moulard, B., Chaigne, D. *et al.* (2000) Mutations of SCN1A, encoding a neuronal sodium channel, in two families with GEFS+2. *Nat. Genet.*, **24**, 343–345.
27. Wallace, R.H., Marini, C., Petrou, S., Harkin, L.A., Bowser, D.N., Panchal, R.G., Williams, D.A., Sutherland, G.R., Mulley, J.C., Scheffer, I.E. *et al.* (2001) Mutant GABA(A) receptor gamma2-subunit in childhood absence epilepsy and febrile seizures. *Nat. Genet.*, **28**, 49–52.
28. Baulac, S., Huberfeld, G., Gourfinkel-An, I., Mitropoulou, G., Beranger, A., Prud'homme, J.F., Baulac, M., Brice, A., Bruzzone, R. and LeGuern, E. (2001) First genetic evidence of GABA(A) receptor dysfunction in epilepsy: a mutation in the gamma2-subunit gene. *Nat. Genet.*, **28**, 46–48.
29. Claes, L., Del-Favero, J., Ceulemans, B., Lagae, L., Van Broeckhoven, C. and De Jonghe, P. (2001) *De novo* mutations in the sodium-channel gene SCN1A cause severe myoclonic epilepsy of infancy. *Am. J. Hum. Genet.*, **68**, 1327–1332.
30. Sugawara, T., Tsurubuchi, Y., Agarwala, K.L., Ito, M., Fukuma, G., Mazaki-Miyazaki, E., Nagafuji, H., Noda, M., Imoto, K., Wada, K. *et al.* (2001) A missense mutation of the Na+ channel alpha II subunit gene Na(v)1.2 in a patient with febrile and afebrile seizures causes channel dysfunction. *Proc. Natl Acad. Sci. USA*, **98**, 6384–6389.
31. Cossette, P., Liu, L., Brisebois, K., Dong, H., Lortie, A., Vanasse, M., Saint-Hilaire, J.M., Carmant, L., Verner, A., Lu, W.Y. *et al.* (2002) Mutation of GABRA1 in an autosomal dominant form of juvenile myoclonic epilepsy. *Nat. Genet.*, **31**, 184–189.
32. Haug, K., Warnstedt, M., Alekov, A.K., Sander, T., Ramirez, A., Poser, B., Maljevic, S., Hebeisen, S., Kubisch, C., Rebstock, J. *et al.* (2003) Mutations in CLCN2 encoding a voltage-gated chloride channel are

associated with idiopathic generalized epilepsies. *Nat. Genet.*, **33**, 527–532.
33. Ogiwara, I., Miyamoto, H., Morita, N., Atapour, N., Mazaki, E., Inoue, I., Takeuchi, T., Itohara, S., Yanagawa, Y., Obata, K. *et al.* (2007) Na(v)1.1 localizes to axons of parvalbumin-positive inhibitory interneurons: a circuit basis for epileptic seizures in mice carrying an Scn1a gene mutation. *J. Neurosci.*, **27**, 5903–5914.
34. Sawamoto, K., Wichterle, H., Gonzalez-Perez, O., Cholfin, J.A., Yamada, M., Spassky, N., Murcia, N.S., Garcia-Verdugo, J.M., Marin, O., Rubenstein, J.L. *et al.* (2006) New neurons follow the flow of cerebrospinal fluid in the adult brain. *Science*, **311**, 629–632.
35. Higuchi, M., Iwata, N., Matsuba, Y., Sato, K., Sasamoto, K. and Saido, T.C.-(2005) 19F and 1H MRI detection of amyloid beta plaques *in vivo*. *Nat. Neurosci.*, **8**, 527–533.

Visual screening and analysis for kinase-regulated membrane trafficking pathways that are involved in extensive β-amyloid secretion

Atsuhiro Adachi[1], Fumi Kano[1,2], Takaomi C. Saido[3] and Masayuki Murata[1,*]

[1]*Department of Life Sciences, Graduate School of Arts and Sciences, The University of Tokyo, Komaba 3-8-1, Meguro-ku, Tokyo 153-8902, Japan*
[2]*PRESTO, Japan Science and Technology Agency, 4-1-8 Honcho Kawaguchi, Saitama 332-0012, Japan*
[3]*Laboratory for Proteolytic Neuroscience, RIKEN Brain Science Institute, Saitama 351-0198, Japan*

Membrane trafficking is an important cellular process that enables the precise localization of membrane proteins. The disturbance of membrane trafficking results in various disease states. To explore systematically the defects in trafficking pathways that cause these disturbances or disease states, we developed an automated high-throughput fluorescence-based imaging system and carried out visual screening for kinase-regulated trafficking pathways of the cation-independent mannose 6-phosphate receptor (CI-M6PR) in HeLa cells. As the result of our visual screening, which examined the effect of kinase inhibitors and a kinase siRNA library, we identified five kinases (CDC42BPB, PRKACA, PRKACG, GSK3β and CSNK2A1) that regulate CI-M6PR trafficking. Moreover, we focused on Alzheimer's disease (AD) to study the relationship between the five kinases and a disease state. Notably, two trafficking pathways, which were regulated by PRKACG and GSK3β, respectively, induced high levels of secretion of Aβ, the hallmark of AD. In addition, we found that the modulation of GSK3β activity affected the microtubule plus end tracking function of cytoplasmic linker protein-associating protein 2 and resulted in the perturbation of BACE1 localization/trafficking and extensive Aβ secretion. Our systems provide new approaches for the analysis of spatially-regulated membrane trafficking and related disease states.

Introduction

Disorders of membrane trafficking pathways cause the disruption of a various cellular functions and sometimes lead to cell death. However, there are few available analytical approaches that allow the investigation of the causal connections between a disrupted trafficking pathway and the pathogenesis of a disease that arises from this disruption. Localizomics is a new field that provides information about the localization of proteins and lipids, and allows the elucidation of the mechanisms that regulate these processes. Our aim was first to establish a versatile functional screening and analytical system for identifying kinases that regulate the membrane trafficking pathways of specific membrane proteins by using fluorescence image-based visual screening techniques. We would then use this system to elucidate the causal connections between a defective transport pathway and the pathogenic mechanisms of diseases that might be caused by mislocalization of the protein. Protein kinases are the most versatile among the many regulators of membrane trafficking. The kinase network has been studied extensively and kinases are likely to prove powerful tools in the search for upstream or downstream proteins that regulate the trafficking of membrane proteins.

To this end, we focused on the membrane trafficking of the cation-independent mannose 6-phosphate receptor (CI-M6PR) and the causal connections between its mislocalization and Alzheimer's disease (AD). CI-M6PR is involved in the trafficking of a broad range of lysosomal enzymes from the trans-Golgi network (TGN) or the cell surface to lysosomes; it mainly shuttles between endosomes and the TGN (Ghosh *et al.* 2003; Arighi *et al.* 2004; Scott *et al.* 2006). It has been shown that defects in the shuttling of CI-M6PR between endosomes and the TGN result in the perturbation of its localization in the cell and can cause many pathogenic states; for example,

Communicated by: Eisuke Nishida
**Correspondence*: mmurata@bio.c.u-tokyo.ac.jp

DOI: 10.1111/j.1365-2443.2008.01274.x
© 2009 The Authors
Journal compilation © 2009 by the Molecular Biology Society of Japan/Blackwell Publishing Ltd.